Journal of Structural Geology 30 (2008) 1489–1506

Contents lists available at ScienceDirect

Journal of Structural Geology

journal homepage: www.elsevier.com/locate/jsg

Tectonics of Nisyros Island, Greece, by field and offshore data, and analogue modelling

A. Tibaldi [a,*], F.A. Pasquarè [b], D. Papanikolaou [c], P. Nomikou [c]

[a] Dipartimento di Scienze Geologiche e Geotecnologie, Università degli Studi di Milano Bicocca, 20126 Milano, Italy
[b] Dipartimento di Scienze Chimiche e Ambientali, Università degli Studi dell'Insubria, Como, Italy
[c] Department for Dynamic Tectonic and Applied Geology, University of Athens, Athens, Greece

ARTICLE INFO

Article history:
Received 26 February 2008
Received in revised form 14 July 2008
Accepted 1 August 2008
Available online 20 August 2008

Keywords:
Faults
Tectonics
Analogue modelling
Caldera
Nisyros

ABSTRACT

We use new on-land and offshore structural data and scaled analogue models to analyse the fault tectonic pattern at Nisyros Island (Greece), which has an active caldera that shows a complicated network of faults, fractures and volcano-tectonic structures. We measured 157 faults that show dominant dip-slip normal motions along planes mainly striking NE–SW, NNE–SSW, and NNW–SSE. Inside the caldera, dykes, necks and morphometric parameters of volcanic domes, explosion craters and fumarole pits indicate the control by NE-striking discontinuities on magma and gas paths. The NNW- and NE-striking faults bound a major block that underwent repeated downthrow and uplift movements during the late Pleistocene–Holocene. Experiments with scaled models of caldera resurgence and two magma chambers indicate the formation of an hourglass-shaped fault pattern, as seen in plan view, with an asymmetric increase in the fault offset and a widening of the fault divergence towards the volcano flank. All these data suggest that regional fault tectonics and stress state strongly guided magma upwelling and the emplacement of volcanic centres, whereas periodical bulging due to the overpressure of a second magma chamber located northwest of the caldera combined with faulting due to tectonic stresses, can account for the overall deformation field.

1. Introduction

Resurgent calderas form by decompression of a shallow-level magma chamber with roof collapse into the evacuating reservoir (Smith and Bailey, 1968; Lipman, 1984, 1997; Newhall and Dzurisin, 1988) followed by new magma inflation and bulging of the caldera floor (Smith and Bailey, 1968; Henry and Price, 1984; Newhall and Dzurisin, 1988). Extracaldera (peripheral) structures can develop during the resurgence phases, being characterised as radial, scissor-like faults (Newhall and Dzurisin, 1988; Chadwick and Howard, 1991; Troll et al., 2002), although the final overall structure of the caldera depends on the initial structure of the volcano, the regional tectonic influence, the size, depth and shape of the underlying magma chamber and its pressure variation (Komuro, 1987; Gudmundsson, 1988; Martí et al., 1994, 2000; Acocella et al., 2000; Roche et al., 2000; Walter and Troll, 2001). Extracaldera structures are a common phenomenon in multicycle caldera systems (Varnes, 1963; Smith and Bailey, 1968; Gardeweg and Ramirez, 1987; Newhall and Dzurisin, 1988; Henry and Price, 1989; Nappi et al., 1991), but their development as related to intracaldera structures remains poorly understood. It has been demonstrated that in some cases the deformation pattern may be complicated by a regional tectonic stress field that controls the elongation of intracalderic resurgent horsts, but also possibly guiding the geometry of extracaldera faults (Bailey et al., 1976; Lipman, 1984; Self et al., 1986).

A common difficulty in studying the evolution of calderas and resurgent calderas is represented by distinguishing between different structural processes, as many calderas are blanketed by extensive covers of pyroclastic fall deposits or filled with thick ignimbrite sequences, hindering detailed measurements of fault and fracture fields. At Nisyros Island, located in the easternmost sector of the Hellenic Arc, Greece (Fig. 1), a 4-km-wide caldera depression shows hundred-metre-high magnificently exposed rock walls and a complex pattern of extracaldera and intracaldera structures, comprising faults, fractures and volcano-tectonic structures such as necks, dykes, craters, volcanic domes and fumarole pit fields. Due to the very dry climate, which does not favour the growth of vegetation, tectonic structures can be tracked in the field. Several outcrops are also exposed by the sea erosion along the coast. In the present paper we integrate detailed field data collected on Nisyros Island, scaled analogue experiments simulating a multicycle caldera volcano with different magma

* Corresponding author.
E-mail address: alessandro.tibaldi@unimib.it (A. Tibaldi).

0191-8141/$ – see front matter © 2008 Elsevier Ltd. All rights reserved.
doi:10.1016/j.jsg.2008.08.003

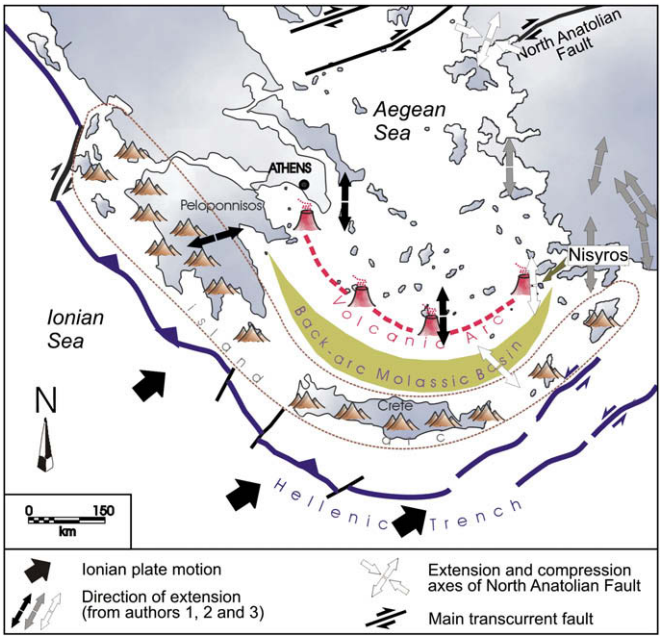

Fig. 1. Simplified map of the present day geodynamic structure of the Hellenic Arc, showing the position of Nisyros Volcano, active volcanic arc, Aegean island arc and Hellenic trench. Extension directions refer to late Quaternary faults from marine data (1: Piper and Perissoratis, 2003), and active faults from earthquakes (2: Jackson, 1994; 3: Hatzfeld, 1999; Papazachos et al., 2000 and references therein).

chamber positions, and offshore structural data, to evaluate the structural implications of fault systems peripheral to calderas and studying their relationship with intracaldera structures and regional faults. A comparison of the various types of onshore and offshore structures with the experimental results helps to elucidate the origin of fault tectonics at Nisyros, to assess the hazards posed by this active system, and to provide a model for investigating other multicycle calderas elsewhere in the world.

2. Background of Nisyros

2.1. Geodynamic setting

The development of the Hellenic Volcanic Arc is the result of the subduction of the East Mediterranean oceanic lithosphere below the European continental plate, at least during the last 45 Ma (Papanikolaou, 1993). The present day geodynamic structure of the Hellenic Arc (Fig. 1) includes the Hellenic Trench, which is a 1500-km-long arcuate trough extending from the Ionian Sea in Western Greece to the Lybian Sea, south of Crete and ending southeast of Rhodos Island. It also includes the parallel structures of the Peloponnese–Crete–Dodekanese island arc and the back-arc mollasic basin of the Cretan Sea. Finally, the Aegean island arc is developed parallel to the Hellenic Trench in a more internal position along the islands to the north of the Cretan basin.

Recent volcanoes occur on Soussaki, Methana, Aegina and Poros to the west, on Milos and Santorini in the centre and on Kos and Nisyros to the east. Submarine volcanoes have also been found in the Epidauros Basin in the western Saronikos Gulf (Pavlakis et al., 1990). The volcanoes of the Hellenic Arc were especially active in the Late Pleistocene–Holocene, with some eruptions known in historical times (Fytikas et al., 1976; Liritsis et al., 1996).

The eastern sector of the Hellenic Volcanic Arc, including the islands of Kos, Yali and Nisyros, resulted from the northeastward-directed subduction of the Eastern Mediterranean lithosphere below the active Hellenic margin of the European plate. It is a very active sector, featuring the largest volumes of volcanic products in Late Pleistocene–Holocene times. Major magmatic activity began at least 0.16 Ma ago (Keller et al., 1990), producing the largest eruption in the Eastern Mediterranean represented by the "Kos ignimbrite", which covered an area of more than 3000 km^2. The centre of this eruption is not known with accuracy but it is probably located in the submarine area north of the Yali islet, a few kilometres northwest of Nisyros (Nomikou, 2004).

2.2. The geology of Nisyros

The island of Nisyros is exclusively made of Quaternary volcanic rocks, represented by alternating lava flows, pyroclastic layers and more viscous lava domes, ranging in age from 200 to 25 ka. Nisyros forms a truncated cone with a base diameter of 8 km and a central caldera, 4 km in diameter. Basement rocks made of carbonates and marbles were found at depth of −600 m in a well located in the northwestern part of the caldera and at −1000 m below the southeastern part by geothermal drillings (Geotermica Italiana, 1983, 1984). The infilling of the caldera above this basement is made of lacustrine, alluvial and tephra deposits. The evolution of this volcano has been described first by Martelli (1917), Desio (1931), Davis (1967) and Di Paola (1974), and more recently it has been divided into five major stages (Papanikolaou et al., 1991; Nomikou, 2003; Vanderkluysen et al., 2005; Volentik et al., 2005): (1) an underwater volcano, with erupting basaltic and andesitic pillow-lavas, built up the lower volcanic rocks visible on the northern coast near Mandraki; (2) A 500–700 m high stratovolcano grew on top of these partly submarine lavas for a period of more than 100 ka; (3) after several eruptive phases of gas and steam explosions, two major rhyodacitic plinian eruptions covered the whole island with pyroclastic flows and pumice falls; (4) subsequently, a major central, vertical collapse of the volcano leaved a large caldera at <20 ka BP (Limburg and Varekamp, 1991); and (5) during pre-historic times, the western part of the caldera depression was filled with a series of rhyodacitic domes, the highest of which, Profitis Ilias, rises 698 m a.s.l.

No volcanic activity is known to have occurred on the island after the formation of the domes for at least 25 ka; the only reported historical explosions are related with the formation of several phreatic craters inside the caldera, such as Alexandros, Polyvotis, Stephanos, Phlegethon and Achelous, which are still emitting fumaroles. Violent earthquakes, gas detonations, steam blasts and mudflows accompanied the most recent hydrothermal eruptions in 1871–1873 and 1887 AD (Marini et al., 1993). During this activity some people were slightly injured and minor damages were caused to the houses.

2.3. Previous studies on the island tectonics

Previous studies have revealed that faults at Nisyros have a radial pattern and are more abundant in the northwest part of the island, where volcanic domes are also concentrated (Papanikolau et al., 1991; Stiros, 2000). Vougioukalakis (1993) recognised three main fault directions (NE–SW, NW–SE and E–W) related to a least principal stress ($\sigma 3$) trending from N–S to NW–SE. Stiros (2000) notes that most faults have a short length and a "scissors-type" geometry typical of magma or salt ascent dynamics, and variable throws that are too high to reflect simply tectonic effects. He suggested that the radial fracture pattern can be explained if faulting is a secondary effect of volcanic doming. Similarly, elevated coastal marine fossils in the northwest of the island indicate rates of uplift too high to be explained solely in terms of differential plate tectonic-related fault movements.

Other information on faults comes from the geological maps of Nomikou (2004) and Volentik et al. (2005). Both studies indicate the presence of several normal faults cutting through the caldera floor with a NE–SW strike. Nomikou (2004) indicates that a main fault striking NNW–SSE, known as the Mandraki Fault, extends southward into the caldera, whereas according to Volentik et al. (2005) this fault stops before reaching the northern caldera rim. A more detailed structural study has been performed by Caliro et al. (2005), but it is limited to a sector of the caldera floor. These authors document the presence of NE-striking normal faults and veins.

Some studies on offshore tectonics have also been carried out around Nisyros (Nomikou and Papanikolaou, 2000; Piper and Perissoratis, 2003; Pe-Piper and Piper, 2005; Pe-Piper et al., 2005) showing that important submarine faults are present in the area. The most significant of these is the northern prolongation of the NNW-striking active Mandraki Fault. Its offset, estimated by submarine profiles, is 100 m and its length is approximately 5 km. Most of the other faults recognised in the basins around Nisyros strike NE–SW and E–W and border some tectonic grabens.

After several years of repose, an intense seismic activity started at the end of 1995 and lasted up to 1998, with the largest event recorded on 27 August, 1997 with a Ms = 5.3 (Papadopoulos et al., 1998). Evidence from seismicity and SAR interferometry suggests that the presently active part of the Kos–Nisyros volcano-tectonic complex is located at the NW coast of Nisyros Island, and that most uplift deformations occurred in the northwestern flank of the volcano (Sachpazi et al., 2002; Lagios et al., 2005).

3. New structural field data on Nisyros

3.1. Methods

We studied in the field several structural features to determine the deformation pattern of the island. Fault field mapping was based on the recognition of polished fault planes, offset stratigraphic markers, or morphostructural evidence of the presence of a fault scarp where outcrops are limited. We applied the Tibaldi (1996) criteria for distinguishing between slickensides on fault planes produced by effective tectonic slip from textures produced by lava segments moving at different velocities within the lava flow. This might help to explain the main differences with the previous structural maps. Data comprise the precise fault location, recorded by a portable GPS, and the measurement of strike, dip, inclination, kinematic indicators on the fault planes and offset amount based on offset markers, wherever possible. Each major fault on the island has been mapped by tracking it in the field. Coeval fault slickensides occurring in an area with a radius $<$100 m have been processed with the Angelier (1990) numerical method to reconstruct the stress tensor.

Fractures are here defined on the basis of the lack of visible offset. In order to process only data on post-emplacement deformation, the measured fracture population contains only values of planes crossing more than one depositional unit; hence, the structures related to the cooling of volcanic units or to soft deposit (i.e. pyroclastic) lithostatic compression have not been included. Moreover, in order not to include in the data set fractures caused by local gravity forces, planes parallel to the slope and located at a distance $<$50 m have not been measured. The dilation direction has been computed as the average direction perpendicular to joint planes measured in a rock wall of 50 m in length, assuming that vertical parallel joints result from pure extension (Pollard and Aydin, 1988).

Other studied structural features comprise dykes, necks and morphometric parameters of volcanic domes, explosion craters and fumarole pits. Dykes have been measured by strike, dip, inclination and thickness, whereas necks have been studied by recognising the classical magma flow indicators in the field, such as phenocrysts, vesicles, laminations, apophyses, grooves, lobes, etc. The study of the morphometric parameters of volcanic features is an indirect methodology to reconstruct magma-feeding paths and can be particularly useful in areas where an extensive cover of volcanic and epiclastic deposits prevents the identification of structures of the volcanic substrate (Tibaldi, 1995; Corazzato and Tibaldi, 2006). Such a methodology allows the definition of the magma-feeding systems and to reconstruct the tectonic evolution of a region or a more limited area. With the general term "substrate" we refer to the base onto which a volcanic feature was emplaced, regardless of its size. These features can be pyroclastic cones (Tibaldi, 1995), volcanic domes (Pasquarè and Tibaldi, 2003) or sinkholes, pit holes, etc. The general view is that dykes propagate across the volcano parallel to the maximum horizontal compressional stress (σH_{max}), forming aligned parasitic cones (Nakamura, 1977). Similar arguments have been used to infer the σH_{max} from the alignment of volcanic centres (e.g. Johnson and Harrison, 1990; Strecker and Bosworth, 1991). Tibaldi (1995) instead introduced nine new morphometric parameters, putting emphasis on the use of morphological features of a single monogenetic cone to infer magma-feeding fracture geometry, rather than on the alignment of cones. At Nisyros we used the following parameters expressed in terms of azimuth, all of which are parallel to the geometry of the underlying magma-feeding fracture: (i) strike of the axis of maximum crater elongation; (ii) strike of the axis of maximum edifice base elongation; (iii) strike of the line connecting the crater-rim depressed points; (iv) alignments of the centre points of coeval craters.

3.2. Faults and fractures

We identified and measured 8 major fault zones (offset $\geq$5 m); we also measured 157 minor faults (offset $<$4 m) and 105 fractures. Sites of measurements are distributed homogeneously both from a spatial point of view and along the entire rock succession (Figs. 2–4). Major faults have throws up to $>$108 m and are generally expressed by multiple parallel fault planes (fault zone). All the major faults have dip-slip motions with normal offset. They strike NE–SW, NNE–SSW and NNW–SSE in order of decreasing frequency (Fig. 5A). Their detailed description, based on numbering in Fig. 2, follows:

F1 It is located along the central part of the caldera (Fig. 2). It is one of the most important fault zones with a N50° strike and a 70–80° dip to the SE (Figs. 6 and 7). Its total throw, given by the sum of the throws of the various parallel fault planes, reaches 100 m. Judging by the lithostratigraphic units cut and offset by this fault zone, we can conclude that it has been reactivated repeatedly, also after the extrusion of Profitis Ilias lavas. Also the most recent deposits are here cut by faults striking NE–SW.

F2 This fault zone is located along the southern caldera wall roughly 1 km southeast of F1; it strikes N50° and dips 70–80° to the WNW. Its total offset may be estimated $>$100 m, although prudence is required because there could be the influence of slip due to the caldera ring fault that locally coincides in strike.

F3 This fault zone, passing through the Mandraki village, is located in the northwestern part of the island and strikes N146° with dips of 75–85° to the NE. It juxtaposes different formations both within and outside the caldera. Offset morphotectonic and stratigraphic indicators point to a throw $\geq$108 m.

F4 This zone is exactly parallel to F3 striking N146°. Faults also here dip to the NE with throw $\geq$50 m. Together with F3, they define a step-like fault arrangement that gradually lowers the

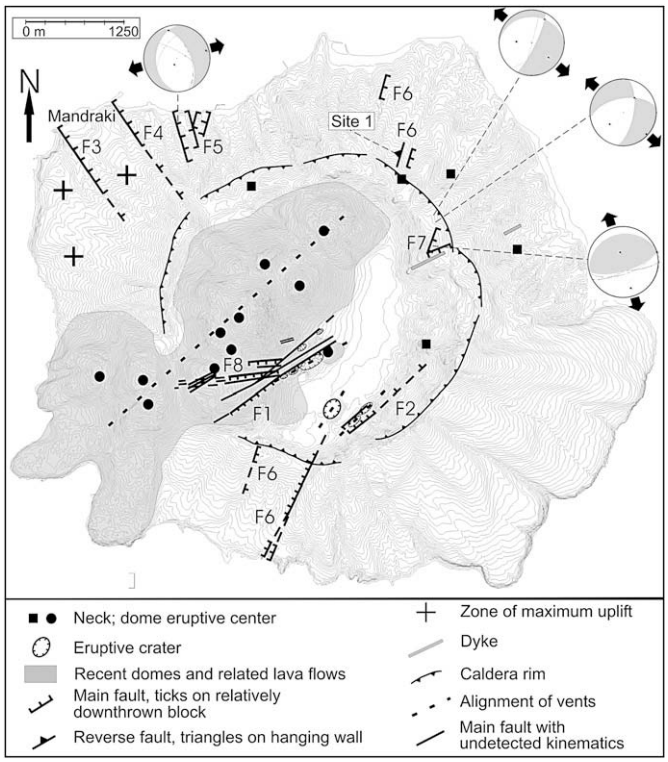

Fig. 2. Map of the main faults, eruptive centres, dykes and necks studied in the field. Note that the majority of faults strike NE to ENE and NNW. Faults show a larger component of normal dip-slip. The dashed line indicates the main alignment of the recent (Holocene) volcanic domes. Stress tensor solutions (black arrows) are given for some selected fault sets where slickenside lineations are present. White arrows show the computed dilation directions based on the normal to the average strike of vertical dilation fractures.

stratigraphic markers to the NE. The scarp height rapidly decreases approaching the caldera rim.

F5 In this zone two fault sets are closely spaced. One set strikes N163°, dipping 55–60° both to the ENE and WSW; the other set strikes N20°, with a dip of 50–85° both to the ESE and WNW (in both fault sets converging dips create small grabens).

F6 This zone is characterised by faults striking N20° with vertical dip. They are present outside the caldera rims and tend to offset the pre-caldera stratigraphic units. At the southwestern volcano flank, these faults have offsets from a few metres to some tens of metres and show converging dips. At the opposite, northeastern volcano flank, the faults have small offsets, in the order of metres, and mostly dip ESE.

F7 This zone has a series of faults belonging to two sets: one striking once again N20° and dipping to the ESE, and the other one striking N70° and dipping to the SSE. Offsets are in the order of tens of metres and dips of 75–85°.

F8 In the western part of the caldera floor there is a swarm of N80°-striking normal faults, dipping 80–90° to the South. The topographic surface is offset in the order of a few metres, suggesting the young age of the faults. In the field, they can be followed from the main NE-striking faults F1 to the western caldera rim. It is important to highlight that these faults are limited to the caldera floor.

Minor faults have centimetric to a few metre offsets; most of them are dip-slip faults with normal offset, with pitches of slickenside lineations ranging from 55° to 86°. Fault strike is dominantly NE–SW and subordinately NNE–SSW and NNW–SSE, with dips of 35–90° (Figs. 3 and 5B). The NNE- and NE-striking fault sets are widespread all over the island; the NNW-striking set is present above all in the northwestern part of the island and in the southern part; the ENE-striking set is more limited to the northeastern part. At site 1 (Fig. 2), we found a swarm of compressional structures with faults dipping 70–85° to the WNW. Striae indicate reverse left-lateral movements, with a series of decimetric drag folds located along the slip planes, with NNE-trending axes (Fig. 5C).

The computed stress tensors (Fig. 2) show a dominant NW–SE-trending $\sigma 3$ and a vertical greatest principal stress ($\sigma 1$). At site 1 (Fig. 2), the $\sigma 1$ is horizontal, trending NW, whereas the $\sigma 3$ is vertical.

The 105 measured fractures show NE–SW, E–W, NNW–SSE and NNE–SSW strikes, in order of decreasing frequency, mostly with vertical dip (Figs. 4 and 5D). The computed dilation directions show a dominant axis trending NW–SE, followed by other more spread directions (Fig. 2).

Summarising the above, the structure of Nisyros is characterised by a series of blocks, each with a relative uplift-horst or relative subsidence-graben. The largest offsets have been recorded at the NE-striking and NNW-striking faults, whereas the NNE- and ENE-striking faults have offsets one order of magnitude lower. Among the largest faults, the NE-striking structures affect the caldera zone (Fig. 6), whereas the NNW-striking faults are limited to the northwestern extracaldera zone.

3.3. Subvolcanic features: Dykes and necks

The structural analysis of the subvolcanic bodies in the island indicates the presence of only two certain dykes, with strike N62°, dip 90° and thickness 1 m (Fig. 2), whereas several morphostructures resembling eroded dyke walls are instead flow structures within very viscous lava flows. Both dykes are located exactly along a main NE-striking zone, crossing the entire caldera floor, where the largest concentration of main NE-striking faults and volcanic centres is found. In this zone some necks occur, three of which have been studied in detail. The field indicators of magma kinematics show an upward-directed flow along dominant NE–SW to ENE–WSW planes, although some dispersion is present (Fig. 5E).

3.4. Craters, domes and fumarole pits

Several volcanic centres are present in the island (Fig. 2). They comprise eroded centres, mostly located along the caldera walls and in the extracaldera volcano flanks, and younger centres located on caldera floor. The latter have been studied with morphometric parameters due to the very good conservation of the original edifice shape. They comprise five explosion craters, 10 volcanic domes and several fumarole pits. The craters (Fig. 7) are concentrated between the domes and the southern caldera wall. They result from hydromagmatic explosions and have been dated at pre-historic to historical times (Caliro et al., 2005, and references therein), thus their original morphology is intact. The base of the edifices show N45–59° major axes, the crater major axes are N36–60° and the crater depressed points trend N58–60° The alignment of these craters is N42–59°. The volcanic domes grew in a zone extending from the southwestern volcano flank to the caldera northeastern part. They show two dominant elongation trends: N–S and NE–SW; however, since they have been emplaced in contact with each other, the N–S elongation can be regarded as due to the morphology acquired when the dome grew buttressed by the pre-existent edifice. As a whole, the 10 recent domes show a N45° alignment.

A field of fumaroles is located on the caldera floor, inside Stephanos crater (Fig. 8). Most gases are emitted by fractures directly cropping out or by vents whose formation is similar to the evolution of tectonic sinkholes produced by erosion processes along

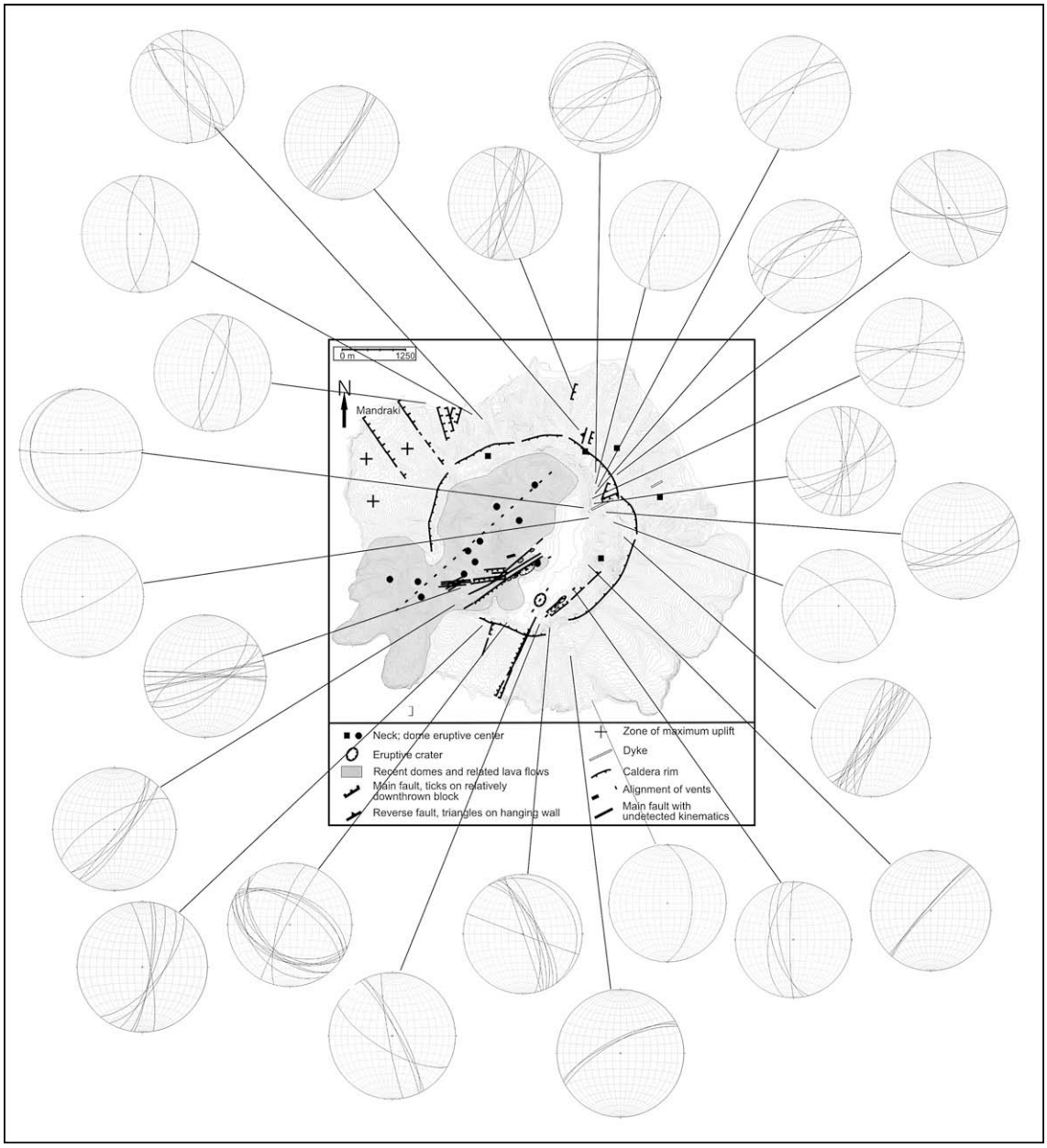

Fig. 3. Schmidt stereograms (lower hemisphere) of the faults without slickenside lineations, superimposed on the map of the main faults, eruptive centres, dykes and necks studied in the field. Note that the majority of faults strike NE to ENE and NNW.

fractures and fissures (e.g. Tibaldi and Groppelli, 2002). Most of the fumarole vents are elliptical in plan view; the strikes of their major axis show two peaks, one at N30° and the other at N100°.

4. Offshore tectonic data

The morphotectonic analysis of a swath bathymetric map (Nomikou, 2004) enabled the detection of the major tectonic faults and the distinction of large basins around Nisyros (Fig. 9). Two main fault zones characterise the whole area: One to the north, forming the southern border of the Kos horst and the other to the south forming the northern boundary of the Tilos horst. In both cases, the major faults have NE–SW and E–W strikes and converging dips. These two major fault zones border a main tectonic depression running with a NE–SW trend, in the axis of which the Nisyros volcano is located, named Nisyros graben. The bathymetric data suggest that this graben formed by a subsidence of the order of 2.5 km. Within the graben, there are a number of faults that are limited mainly to the central part of the area, creating a minor internal horst that is better expressed in the area of Kondeliousa islet. A few of these faults can be classified as major faults based on their length (several kilometres long) and their escarpment heights, which are in the order of tens to hundreds of metres. Such major faults are observed mainly on both sides of the Kondeliousa rise with a NE to ENE strike. The total amount of subsidence produced by all these faults is of several hundred metres on both sides of Kondeliousa islet. Thus, Kondeliousa forms an important horst structure splitting towards the southeast the Nisyros graben into two parallel, NE-trending grabens.

The analysis of the high-resolution swath bathymetry map permitted the delineation of five distinctive basins: Two basins are distinguished between Kos and Nisyros; the larger and deeper basin of Eastern Kos, with an average sea-bottom depth of 630 m, and the smaller basin of western Kos whose average depth is

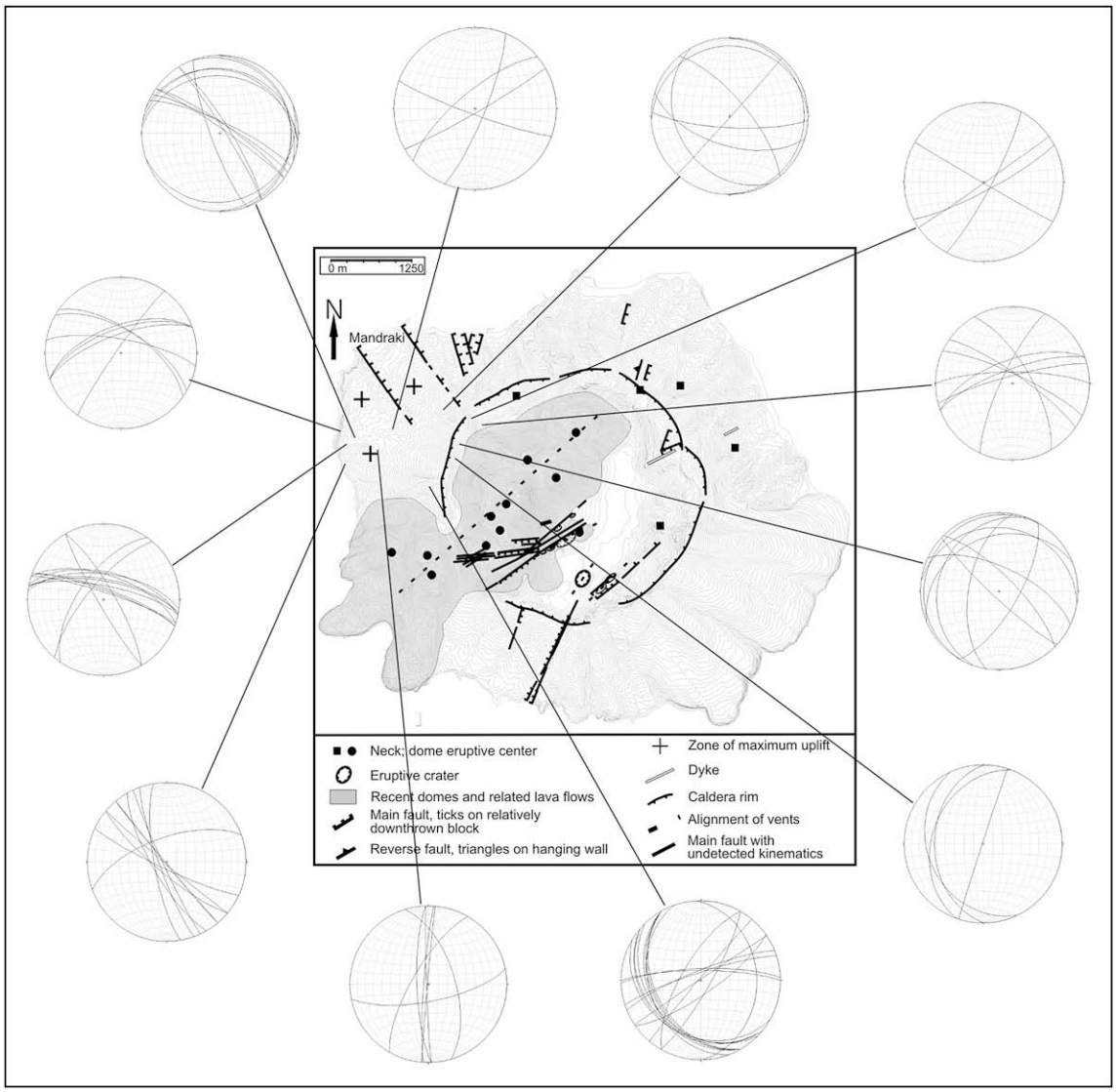

Fig. 4. Schmidt stereograms (lower hemisphere) of the fractures, superimposed on the map of the main faults, eruptive centres, dykes and necks studied in the field. Note that the majority of fractures strike NE to ENE, NNW and other minor sets.

520 m. These two basins are separated by a relatively shallow rise between Yali and Kos with a depth of 400 m.

Analyses of the offshore data indicate that the NE-striking structures have different ages based on the various fault scarp heights across different deposits. An example can be seen in Fig. 9B, where a 3-D view of the southwestern zone offshore Nisyros shows the presence of a NE-striking fault scarp affecting the deposits below the Nisyros Holocene dome lava flows. The same fault is not detectable in the offshore Holocene dome lava flows, suggesting that large motions along this fault mostly occurred before the dome emplacement.

5. Analogue modelling

5.1. Scaling procedure

The experimental device (Fig. 10) we used is located in the "Volcano-tectonics Lab" at the University of Milan Bicocca; it consists of a scaled volcano–caldera system, two analogue magma chambers, which have been located at different depth and position with respect to the volcano and an interposed crust (Table 1). The different combinations provided a total of 60 experiments. One magma chamber has been located below the volcano, and a second one to the NNW in different locations. The magma chambers are made of a rubber bladder containing water linked to a manometer. Rubber bladders have been largely used in the past by other authors for mimicking the inflation of magma chambers (Martí et al., 1994; Lagabrielle et al., 2001; Troll et al., 2002; Kennedy et al., 2004). These are a valid simplification of reality, as long as the following conditions are abided by (and this is the case in our experiments): (i) only inflation and deflation are occurring, (ii) no intrusion mechanisms are intended to be modelled, and (iii) essentially the location/geometry of the structures are considered. During each experiment, the volcano has been built complying with the classical scaling procedures (Komuro, 1987; Roche et al., 2000, and references therein) and, after its construction, the previously inflated chamber below the volcano centre has been deflated producing the formation of caldera-related structures. Depth, dimension and deflation amount of the magma chamber have been initially scaled in order to match reasonable values of the real chamber and then slightly adjusted through a series of preliminary experiments in order to have the formation of a caldera with the exact scaled position, shape and dimension with respect to

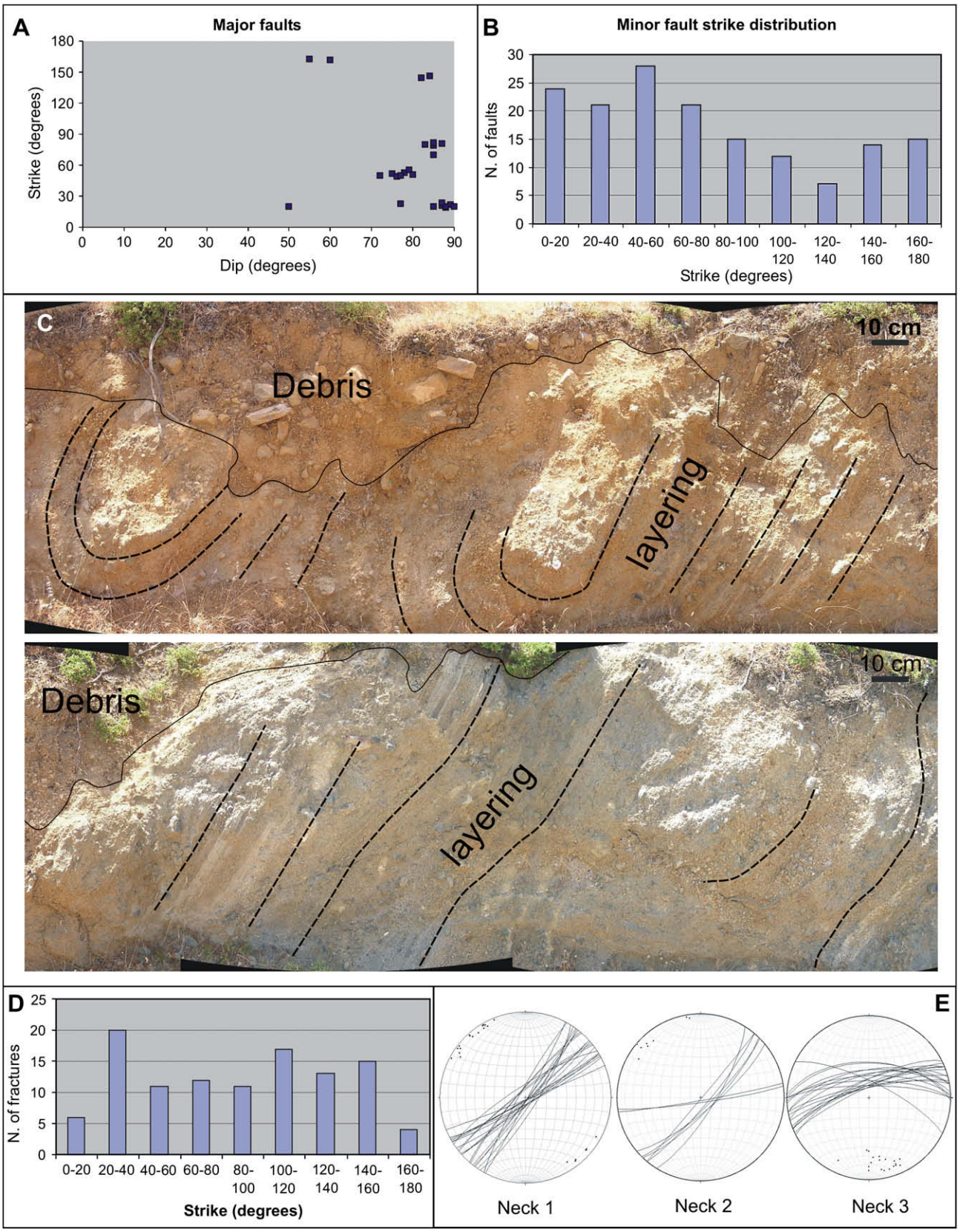

Fig. 5. (A) Graph showing strike frequency of major faults, that is NE–SW, NNE–SSW and NNW–SSE in order of decreasing frequency, with dips ranging from 50° to 90°. (B) Graph showing minor fault strike frequency. It is dominantly NE–SE and subordinately NNE–SSW and NNW–SSE, with dip amount ranging from 20° to 90°. (C) At site 1 (location in Fig. 2), we found a swarm of compressional structures comprising faults dipping 75° to the WNW and decimetric drag folds. Striae indicate reverse left-lateral movements, while the decimetric folds located among the slip planes show axes trending N20–30°. (D) The 105 measured fractures show NE–SW, E–W, NNE–SSW and NNW–SSE strikes, in order of decreasing frequency. (E) In the studied necks, the field indicators of magma flow kinematics show an upward-directed flow along dominant NE–SW to ENE–WSW planes, although some dispersion is present. Neck 1 is located on road from Pali to Emborio. Neck 2 is located SE of Emborio. Neck 3 is located between the Monasteries of Aghios Thelagos and Stàvros.

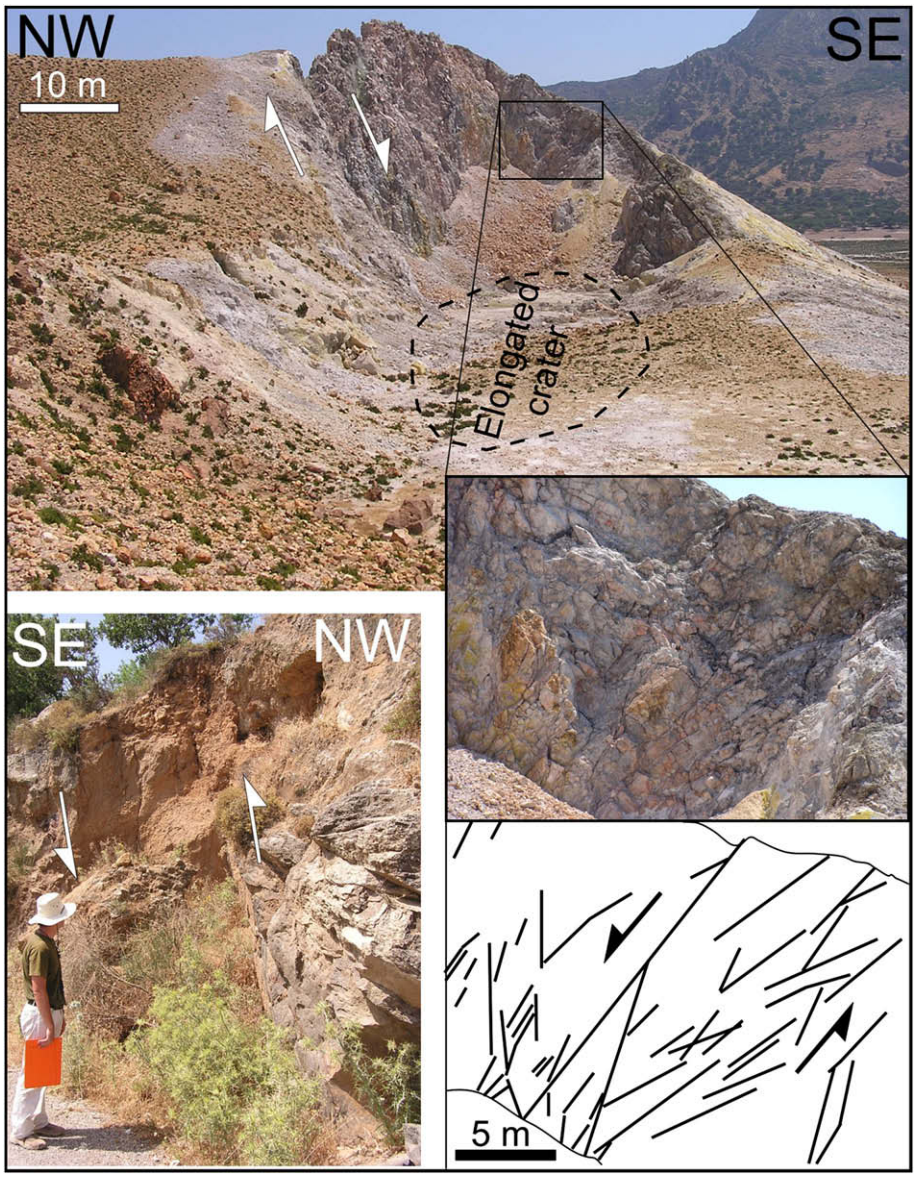

Fig. 6. Examples of faults studied in the field. Above, the main NE-striking fault system located along the northern part of the caldera is shown. Here, one of the main fault dipping towards the SE can be observed. The close-up shows antithetic faults cutting one of the youngest craters in the caldera floor. Below is another fault, also striking NE, found outside the caldera.

Fig. 7. The craters are concentrated between the domes and the southern caldera wall. They resulted from hydromagmatic explosions and have been dated to pre-historic to historical times (Caliro et al., 2005), thus their original morphology is intact. The base of the edifices show N45–59° major axes, the crater major axes are N36–60° and the crater depressed points trend N58–60°.

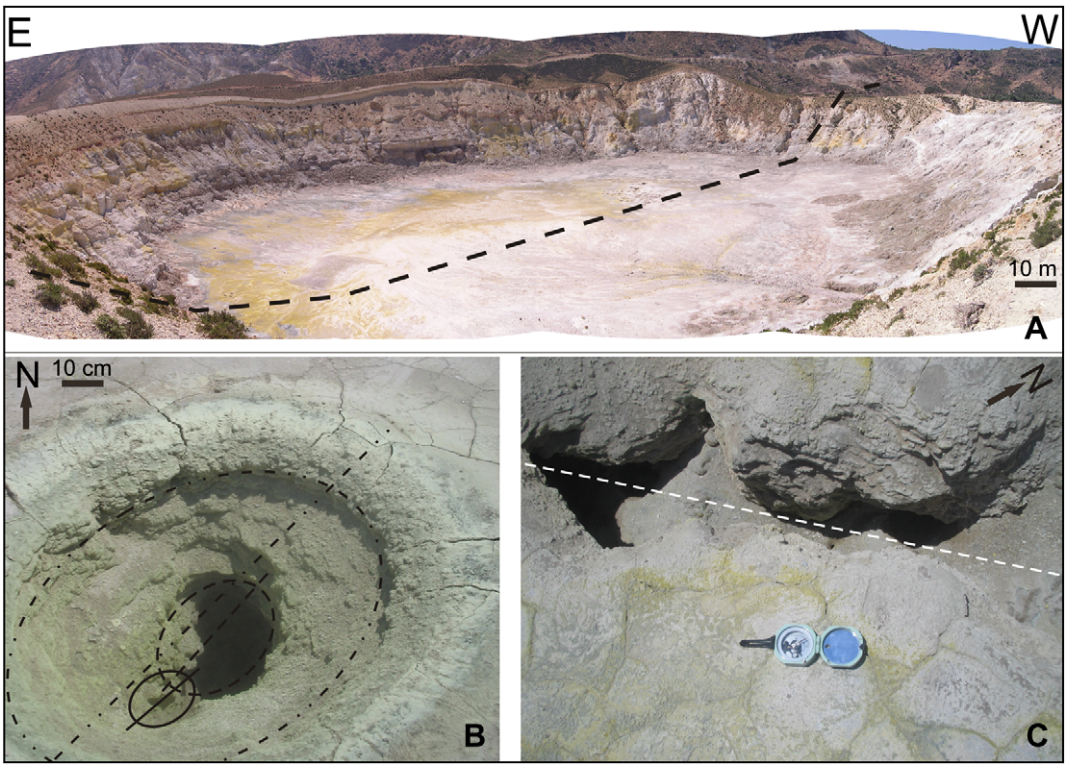

Fig. 8. (A) General view of the largest hydromagmatic crater located in the southern part of the caldera bottom. The dashed line shows the NE–SW elongated axis of the crater. (B) Photo of one of the measured fumarole vents showing the NE–SW alignment of two elliptical holes, and the NE–SW orientation of the major axis of the various holes. (C) Some fumaroles are so strongly tectonically-controlled that they resemble a fissure, such as the one here portrayed that also trends NE–SW.

the real field conditions. Once the caldera was formed, the second chamber was inflated; the location, dimension and volume inflation have been correctly scaled according to the known real parameters (Sachpazi et al., 2002; Sakkas et al., 2002) (Table 1). The inflation was produced with steps of known amount of volume increase of the magma chamber, producing fault deformations at the surface that have been photographed at each incremental steps with a high resolution camera. Fault location, strike, dip, length and offset have been accurately measured at each incremental step for each experiment.

As concerns the scaling procedure, the theory of scale modelling requires that a model, in order to be a valid representation of a natural prototype, is scaled both kinematically and dynamically (Hubbert, 1951; Ramberg, 1981; Troll et al., 2002; Kennedy et al., 2004). A well-developed scaling methodology has been established for tectonic (e.g. Corti et al., 2002; Lohrmann et al., 2003) and volcano (e.g. Tibaldi, 1995; Merle and Borgia, 1996; Lagmay et al., 2000; Vidal and Merle, 2000; Acocella, 2005; Tibaldi et al., 2006) deformations. In order to achieve dynamic similarity, the ratio of gravitational to cohesive forces ($R = \rho g L/C$, where ρ = density, g = gravity acceleration, L = characteristic length, C = cohesive strength) must be the same in the model and in nature ($R_{\text{prototype}}/R_{\text{model}} = 1$; Hubbert, 1951; Ramberg, 1981; Weijermars and Schmeling, 1986). This condition is achieved in natural gravity ($g_{\text{prototype}} = g_{\text{model}}$) choosing the right linear scale factor ($L_{\text{prototype}}/L_{\text{model}}$) as a function of prototype and model material parameters (ρ and C). Under brittle conditions, deformation is not time-dependent provided that inertial forces are negligible (Hubbert, 1951).

Three different analogue materials have been selected (SQS sand, Q100 sand and flour), simulating the main types of volcanic materials observed at Nisyros. For reproducing the substrate we used Ticino River sand (ST), with the same grain-size as SQS, but composed of less rounded grains (higher cohesion). Using these materials (properties listed in Table 2), dynamic similarity is achieved for a linear scaling ratio of 1/25,000. The apical angle of the cone was maintained similar in the model and in nature, in agreement with the principle that angular quantities, being dimensionless, should be equal in the prototype and in the model (Hubbert, 1951).

The used geometric variables are: The height of the volcano (h_v), the ray (r_c) and the depth (d_c) of the caldera, the depth (d) and the ray (R) of the magma chamber; the variables of the materials are the density (ρ) and the cohesion (c). The real values of the materials composing the rock succession at Nisyros have been taken from Krantz (1991), Saotome et al. (2002), Lohrmann et al. (2003) and Apuani et al (2005). In accord with the Buckingam-Π Theorem (Bird et al., 1960, p. 85), the seven considered variables less the two dimensions determine a total of five adimensional parameters that must be equal between the experiment and the prototype. Four dimensional parameters represent the geometric relationships of the system:

$$\prod 1 = \frac{\text{volcano height}}{\text{caldera ray}} = \frac{h_v}{r_c};$$

$$\prod 2 = \frac{\text{caldera depth}}{\text{caldera ray}} = \frac{d_c}{r_c};$$

$$\prod 3 = \frac{\text{magma chamber ray}}{\text{caldera ray}} = \frac{R}{r_c};$$

$$\prod 4 = \frac{\text{magma chamber depth}}{\text{magma chamber ray}} = \frac{d}{R}.$$

The last adimensional value is related to the material properties:

$$\prod 5 = \frac{\text{stress}}{\text{cohesion}} = \frac{\rho g r_c}{c}$$

where g is the acceleration of gravity.

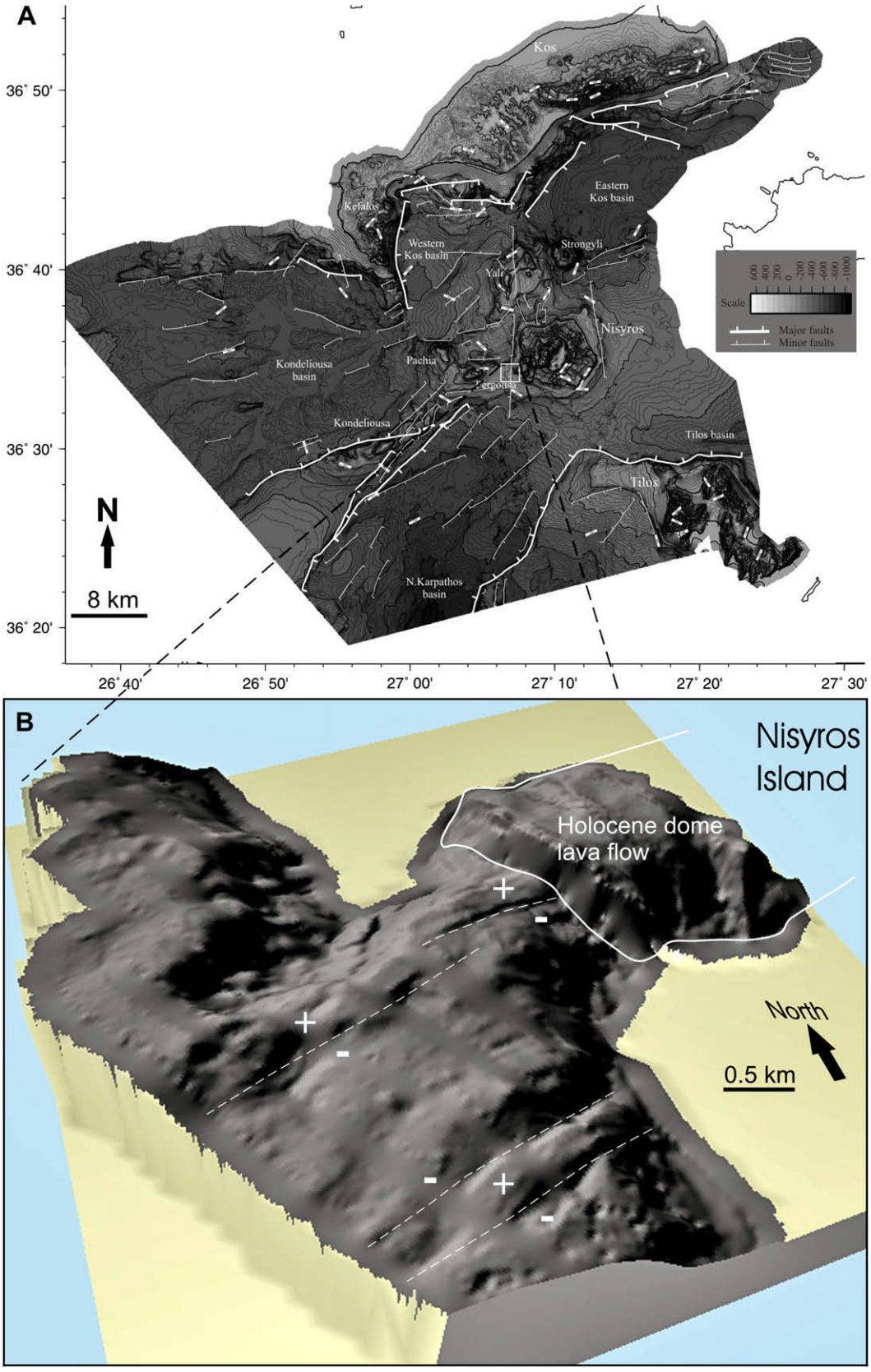

Fig. 9. (A) Bathymetric map of the area surrounding Nisyros. Note the main systems of faults striking mostly NE–SW and subordinately E–W. Faults show a dominant component of normal motions, as well as the majority of graben and horst structures trend NE–SW. These data indicate that the regional tectonics surrounding Nisyros island has been characterised by a large component of extension with a possible dominant NW–SE-trending axis. The NE–SW-trending zone of weakness crossing the island is compatible with the findings all over the area studied by marine geology. (B) 3-D view in detail of the southwestern zone offshore Nisyros (location in A). Note the NE-striking fault scarps mostly preceding the Holocene dome lava flow.

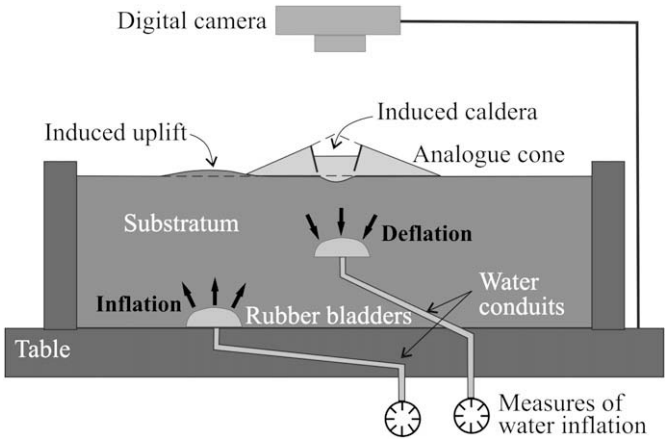

Fig. 10. Sketch (not to scale) of the apparatus used for the experiments; it consists of two analogue magma chambers which have been located at different depth and position with respect to the scaled Nisyros volcano. One magma chamber has been located below the volcano, and a second one further to the NNW in different positions (see also Table 1). The magma chambers are made of a rubber bladder containing water connected to a manometer. During each experiment, the volcano has been built respecting scaling procedures and after its construction, the previously inflated chamber below the volcano centre has been deflated producing the formation of the caldera structures. Successively, the other magma chamber has been inflated.

Table 1
Main characteristics of the experiments

Height of the volcano from the sea bottom (h_v)	2.5 cm (1 km)
Ray of the caldera on the volcano (r_c)	5 cm (2 km)
Depth of the caldera on the volcano (d_c)	0,8 cm (0.32 km)
Depth of the magma chamber below the volcano (d)	20 cm (8 km)
Ray of the magma chamber below the volcano (R)	5 cm (2 km)
Volume increase of the offshore magma chamber	15.5%, 22.5%, 29.5%
Depth of the offshore magma chamber	From 18.5 cm (7.4 km) to 21.3 cm (8.5 km)
Plan view distance of the offshore magma chamber from the northern caldera rim	From 8,2 cm (3.3 km) to 14,2 cm (5.7 km)
Azimuth of the offshore magma chamber with respect to the centre of the Nisyros caldera	From N60° W to N30° W

In nature $h_v = 1000$ m (inclusive of the submerged part of the volcano), $r_c = 2000$ m, $d_c = 320$ m, $R = 2000$ m, $d = 8000$ m (Sachpazi et al., 2002; Sakkas et al., 2002), $\rho = 2.6$ g/cm^3 (weighted average) and $c = 105$–106 Pa. The parameters for the prototype are: $\Pi 1 = 0.5$, $\Pi 2 = 0.16$, $\Pi 3 = 1$, $\Pi 4 = 4$ and $\Pi 5 = 10^2$. In this way it has been possible to calculate the values of the scaled model: $h_v{}^* = 2.5$ cm, $r_c{}^* = 5$ cm, $d_c{}^* = 0.8$ cm, $R^* = 5$ cm, $d^* = 20$ cm, $\rho^* = 1.35$ g/cm^3 and $c^* = 25$ Pa. Each scaled incremental step of inflation of the magma chamber located NNW of the caldera was of 50 ml, with three volume increases (ΔV) simulated for each experiment, corresponding to a growth of 15.5%, 22.5% and 29.5% respect to the original magma chamber volume.

5.2. Results of the analogue experiments

During variations in the volume of the magma chamber located below the centre of the Nisyros volcano analogue model, the pattern of deformation was dominated by circular ring faults during deflation, corresponding to caldera formation, or circular and radial faults and fissures formation during inflation. None of these preliminary experiments was thus able to reproduce the pattern of extracaldera deformation present on the island. The successive experiments conducted after deflation of the magma chamber below the volcano and inflation of the second magma chamber located NNW, produced a series of faults/fissures peripheral to the caldera.

Fig. 11 shows three representative examples of experiments where the second magma chamber is located at 11.2 cm in plan view from the northern caldera rim (equivalent of 4.5 km) and at 20 cm of depth (8 km, Cases A, B), and at 18.5 cm (corresponding to the uncertainty in the chamber location at 7.4 km of depth, Case C). In all the cases, whatever the inflation percentage, a fault pattern characterised by an asymmetric hourglass-like shape in plan view has been produced (in Case A ΔV is 22.5%; in Cases B and C $\Delta V = 29.5\%$). A swarm of parallel faults and fissures striking NW–SE are along the upward projection of the magma chamber. Here the western faults of this system dip to the NE and the eastern faults dip to the SW, showing converging dips and delimitating a NW–SE-trending step-like graben structure. These fault sets tend to slightly diverge towards the northern part of the system, acquiring a N–S strike in the eastern portion of the swarm and a WNW–ESE strike in the western portion. Towards the southern part of the system, faults and fissures tend to more strongly diverge opening in a fan shape: the western faults bend to acquire a N–S strike, whereas the eastern faults bend to an E–W to ENE–WSW strike. These strikes along the southern part of the system tend to parallel the volcanic cone flanks. It is important to note that along the axis of this fault fan, at least a main NW-striking fault propagates in all the experiments towards the caldera, dipping to the NE. Parallel to this fault there is also a series of minor, shorter faults and fissures. Fissures tend to concentrate above the magma chamber, although in a few cases some fissure propagate in the area external to the magma chamber. To the right side of Fig. 11, we represent also the real coast line of Nisyros with the location of the Mandraki village: We point out that in this series of experiments, the NE-dipping fault passes close to Mandraki. If we observe the pattern of this fault on-land from the position corresponding to the coast line up to the south-eastern tip (i.e. towards the caldera), the scarp height suggests a scissor-type offset along the fault plane.

Faults are from vertical to sub-vertical. Offset is normal along all the faults, corresponding to maximum offset values of 10–40 m in the reality for a $\Delta V = 15.5\%$, 80–120 m for $\Delta V = 22.5\%$ and 200–300 m with $\Delta V = 29.5\%$. Maximum offset values occur along the central part of the faults, above the magma chamber, and rapidly decrease towards the fault tips. Normal offsets mostly correspond to absolute uplift of the footwall rocks, which absorb part of the

Table 2
Physical properties of analogue materials used in the experiments and volcanic rock masses at the studied volcano

	Material	Density (t/m^3)	Cohesion (Pa)	Refs.
Model	SQS sand (0.150–0.210 mm)	1.50	25	a, c
	Q 100 sand (0.100 mm)	1.20	69	a, c
	Flour	1.20	330	a
Prototype	Pyroclastic deposits	2.40	1.E+06	b, d
	Andesitic/basaltic fractured lavas	2.65	5.E+06	b, d
	Andesitic/basaltic poorly fractured lavas	2.65	2.E+07	b, d

References: (a) Krantz (1991) (b) Saotome et al. (2002) (c) Lohrmann et al. (2003) (d) Apuani et al. (2005).

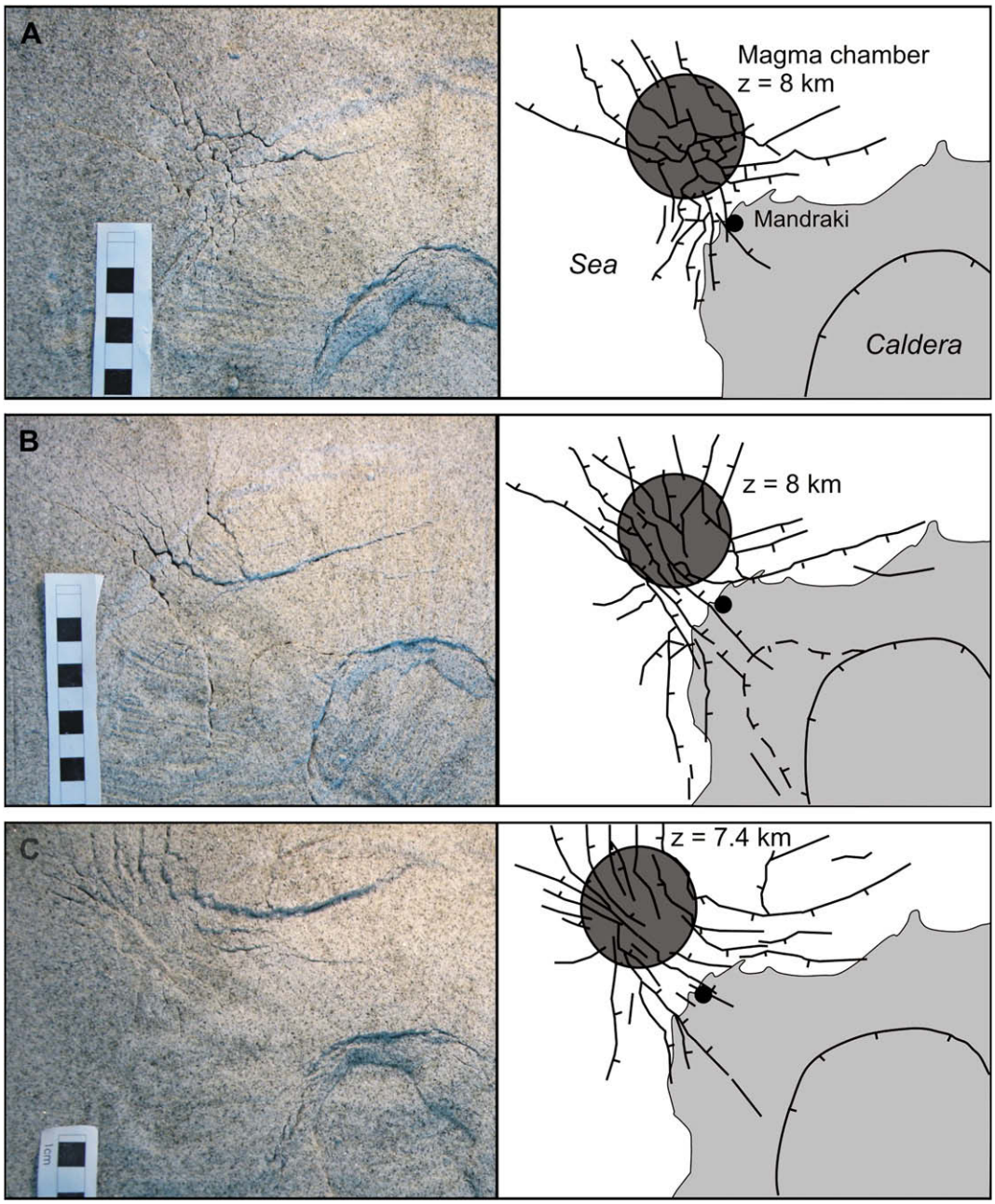

Fig. 11. Photo of three representative examples of experiments where the second magma chamber is located at 11.2 cm in plan view from the northern caldera rim (equivalent of 4.5 km) and at 20 cm of depth (8 km, Cases A, B) and at 18.5 cm of depth (corresponding to the uncertainty in the chamber location at 7.4 km of depth, Case C). In all the cases, whatever the inflation percentage, a fault pattern characterised by an asymmetric hourglass-like shape in plan view has been produced.

deformation linked to the magma chamber inflation. In those experiments where we reached the largest values of ΔV, in some case we had the development of an incipient collapse directed towards the caldera floor (see the arcuate feature in Case B of Fig. 11). In the case of a less deep magma chamber, we have the same fault pattern with an increase in fault offset (e.g. Case C, Fig. 11).

Fig. 12 shows two representative examples of experiments where the second magma chamber is located closer to Nisyros, or it has been placed further to the NE, always maintaining a depth of the magma chamber corresponding to 7.6 or 8 km in the field. In other experiments, not shown here (see also Table 1), the magma chamber has been moved further to the north or to the west. In all these cases, whatever the inflation percentage, the resulting structure is different and tends more to resemble a classical radial fault pattern (Case B, Fig. 12). In case the magma chamber is moved closer to Nisyros, at lower ΔV we obtain the asymmetric hourglass-like fault pattern, but the faults tend rapidly to prolong south-eastward reaching and crossing the caldera wall (Case A, Fig. 12). Also in these cases some fissures develop above the magma chamber, with dominant WNW to NW strikes.

6. Discussion

The study of the structures of Nisyros Island by means of field data, together with the analysis of the offshore structures and analogue modelling, highlights a complex pattern of deformation that could result from different causes. In a resurgent, active caldera

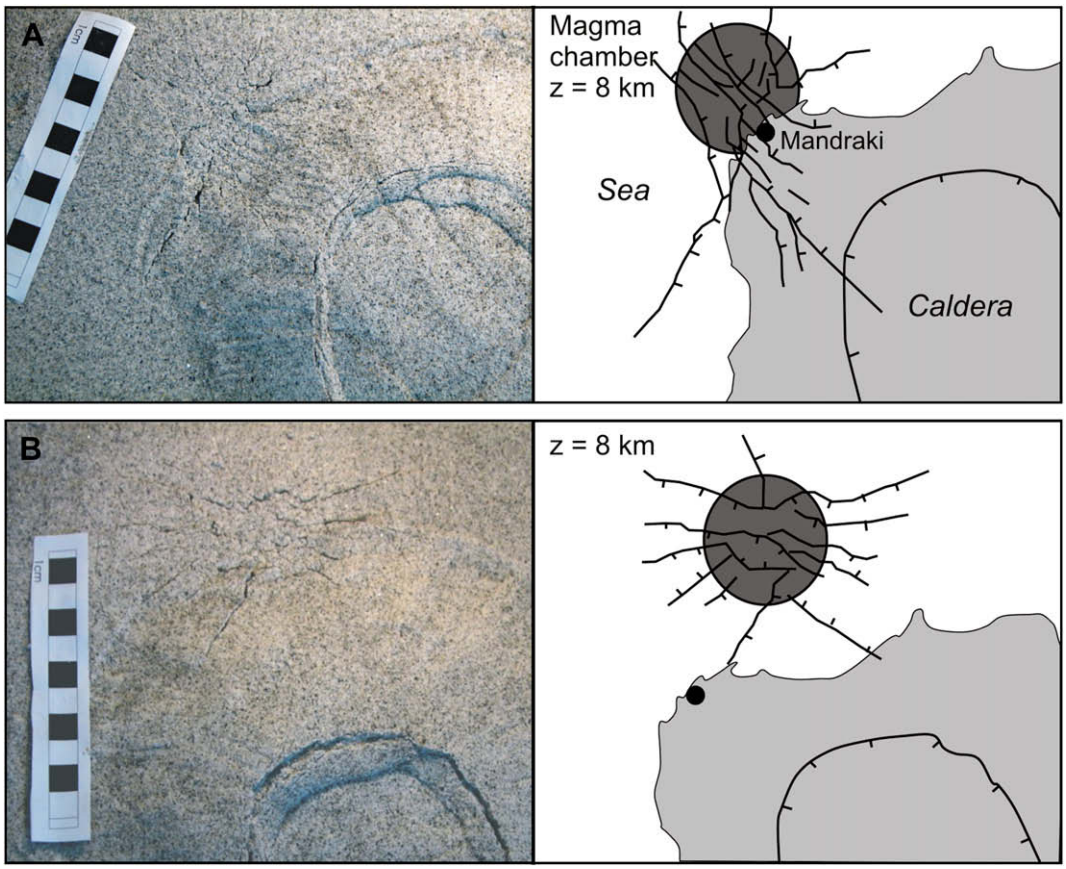

Fig. 12. Photos and interpretations of two representative examples of experiments where the second magma chamber is located closer to Nisyros respect to Fig. 11 (A), or it has been placed more to the NE (B), always maintaining a depth of the magma chamber corresponding to 7.6–8 km in the reality. In other experiments, here not shown, the magma chamber has been moved more to the North or to the West (see also Table 1). In all these cases, whatever the inflation percentage, the resulting structure differs from field data and tends more to resemble a classical radial fault pattern (as Case B). If the magma chamber is moved closer to Nisyros, at a lower magma chamber volume increase we obtain the asymmetric hourglass-like fault pattern but the faults tend rapidly to prolong southeastward reaching and crossing the caldera wall (B).

environment, different types of hazards are present and prudence is required in deciphering the reasons for deformation. Although few calderas have formed during historical times, resurgent calderas are quite common. There have been 1300 episodes of historical unrest recorded at 138 calderas (>5 km diameter, Newhall and Dzurisin, 1988), suggesting the general importance of the studies on post-caldera activity. In the following two sections we will first try to unravel the significance of the NE-striking structures, and then of the other structures.

6.1. The role of NE-striking structures in Nisyros

With a thinner overburden, the post-caldera growth is accompanied by the formation of a crestal depression with radial fractures and extrusion (Acocella et al., 2000). This is due to the development of apical tensile stresses (Gudmundsson, 1999). The formation of crestal depressions was also recognised by Komuro et al. (1984), Davison et al. (1993), Schultz-Ela et al. (1993) and Martí et al. (1994). Radial extensional structures have also been documented during doming experiments (Ramberg, 1981; Withjack and Scheiner, 1982; Dixon and Simpson, 1987; Troll et al., 2002). With a thicker overburden, no deflection of the layers should occur (Roman-Berdiel et al., 1995; Acocella et al., 2000), because it has a higher flexural strength (Turcotte and Schubert, 1982), but an ascending magma diapir intrusion increases the area of deformation and the circumference of the resurgent dome, once again creating radial fractures (Phillips, 1974; Mandl, 1988). It has also been proposed that under certain conditions, regional doming may generate a crestal caldera (Komuro, 1987; Gudmundsson, 1998), but natural cases and analogue and numerical modelling show that a deformation pattern characterised by regional doming have radial faults, fractures and eruptive fissures (Nordlie, 1973; McGuire and Pullen, 1989 and references therein; Chadwick and Howard, 1991; Chadwick et al., 1995; Reynolds et al., 1995).

Our case study shows instead a more complex pattern. Our data show that the Nisyros caldera floor is affected by a swarm of faults and fractures mostly striking NE–SW (N45–55°) and ranging from NE–SW to ENE–WSW (N45–80°) (Fig. 13). Along the southeastern, southern and southwestern volcano flanks, some radial lineaments previously suggested by other authors have been here studied in detail in the field. Our results indicate that these lineaments are not faults but they actually are shear zones linked to lava flow segments moving at different velocities during their emplacement, similar to what has been found elsewhere (e.g. Tibaldi, 1996). The NE–SW structures are the longest features and locally affect also the caldera walls and the extracaldera zones, as witnessed also by the offshore data (e.g. in Fig. 9B). Although the NNE-striking structures previously reported within the caldera appear in the interior of the caldera rim (F7, Fig. 2) they outcrop only on the caldera walls; hence, they should be considered belonging to the footwall of the caldera ring fault and thus extracalderic structures (Fig. 13B). Striae measured on the fault planes indicate a NW–SE-directed least principal stress ($\sigma 3$), consistent with the results of the maximum elongation trend obtained by the analysis of the main fracture sets. The analysis of the morphometric parameters of the explosion craters, domes and fumarole vents shows that they are dominantly

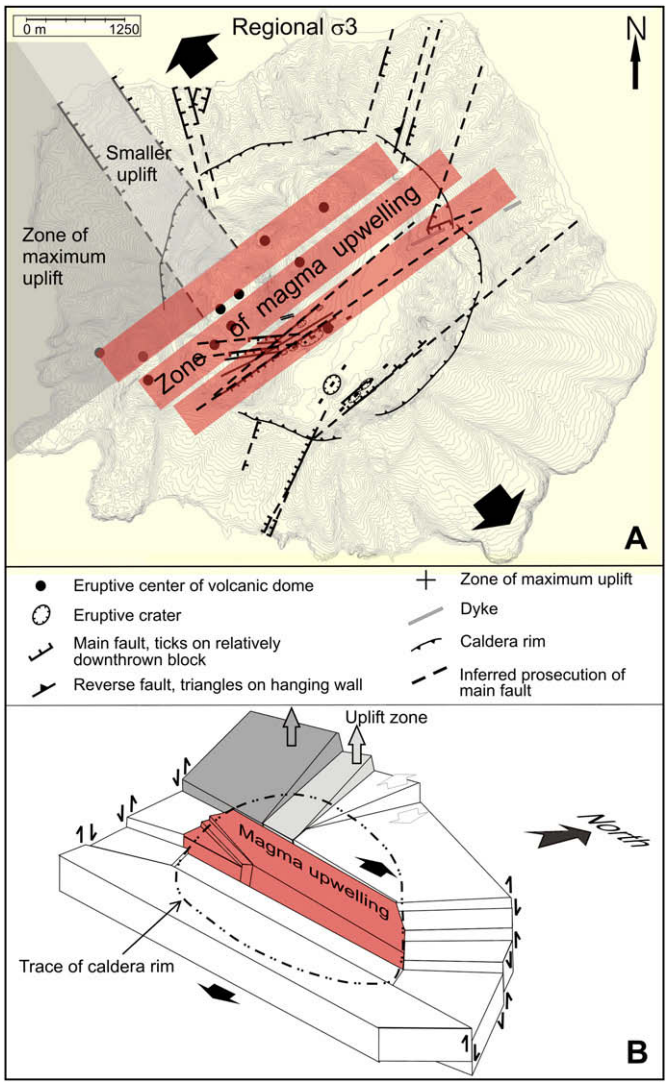

Fig. 13. (A) Sketch on the relationships between the main fault zones, the preferential NE–SW zone of magma injection across the Nisyros island, the location of the long-term uplifted block, and the reconstructed stresses. (B) 3-D sketch of the main tectonic blocks which divide the island. Colours of blocks are the same as A.

controlled by NE-striking fluid paths. Volcano-feeding paths result from the injection of magma along fractures that are better oriented with respect to the stress state of the host rock, being the planes normal to $\sigma 3$ more suitable. At Nisyros, this suggests that the NE-striking magma paths should be those oriented perpendicularly to the $\sigma 3$ acting in the island during magma emplacement. This is also consistent with the findings on veins by Caliro (2005) and with our finding of flow directions in necks along planes striking from NE–SW to ENE–WSW, as well as two dykes striking ENE–WSW. Also the most recent volcanic activity in the island has been dominated by domes, which are aligned NE–SW across the entire caldera floor but also prolong on the extracaldera southwestern area. All these on-land data are consistent with the offshore data showing the presence of NE-striking fault scarps affecting the deposits below the offshore Nisyros Holocene dome lava flows (Fig. 9B). This indicates that large motions along this NE–SW fault zone occurred before the dome emplacement and might have provided the pathways for the dome magma rise.

The coherence of the various types of data, suggests that the caldera area has been subjected to a NW–SE-directed $\sigma 3$ that also controlled the distribution of volcanic vents and magma paths. The presence of NE-striking normal faults cutting across the entire caldera block has also been inferred on the basis of the offset of main stratigraphic units encountered in geothermal wells (Marini et al., 1993).

6.2. Relationship of NE-striking structures with regional tectonics

Looking at the regional data, it emerges that the area surrounding Nisyros is also characterised by the dominant presence of NE-striking faults, together with less abundant E–W-striking faults. Both fault sets show a large component of vertical displacement as can be reconstructed by the bathymetric relief, and are arranged in a series of NE-trending grabens. A number of submarine and island volcanic centres developed within these depressions (Nomikou and Papanikolaou, 2000; Papanikolaou and Nomikou, 2001), most of them being NE–SW-aligned (Tibaldi et al., in press). These data, together with the presence of the grabens, suggest a regional NW–SE-trending direction of extension.

Some authors suggested that the regional Quaternary direction of extension in the southeastern Aegean Sea is N–S (Piper and Perissoratis, 2003; Mountrakis, 2005), while other authors indicated for the same region a NW–SE trend of the regional $\sigma 3$ axis along NE-striking normal faults (Jackson et al., 1982; Papazachos et al., 2005), or normal faulting following a N–S to NW–SE $\sigma 3$ passing from the southeastern Aegean Sea to western Turkey (Jackson, 1994). In an area with a radius of 70 km centred on Nisyros, focal mechanism solutions indicate T-axes trending from WNW–ESE to NW–SE south of the island, from NW–SE to NE–SW to the north, and N–S to the northeast (Hatzfeld, 1999). The same author concludes that a NE-striking normal fault located between Nisyros and Kos might be active. Piper and Perissoratis (2003), on the basis of marine data of eastern Aegean Sea, suggest that Pliocene E–W-striking faults have been replaced about 0.2 Ma ago by ENE-striking left-lateral strike-slip faults, and Pe-Piper and Piper (2005) and Pe-Piper et al. (2005) indicate that more local NE-striking normal faults developed within a left-lateral regime.

This variability of results largely depends on the fact that on-land data are limited to a few islands, reliable crustal focal mechanisms are scarce in the region, and most conclusions are drawn on the basis of interpretation of bathymetric maps. These maps, accompanied by seismic profiles, give very useful indications on fault strikes and the prevailing component of motions, but precise fault kinematics with stress directions of course cannot be obtained. Our offshore data alone in fact, indicate two possible extension directions as suggested by the strike of the two fault sets showing a large component of dip-slip normal motions. If the two fault sets are coeval, one of them should have a component of transcurrence to adjust the extension along the other set. The only field data with fault striae within a reasonable radius from Nisyros, refer to the entire Plio-Pleistocene time window at one locality in Kos island, 18 km north of Nisyros (Doutsos and Kokkalas, 2001) and indicate normal faulting with a NNE–SSW $\sigma 3$. In a wide area south of Nisyros instead, the same authors found a constant NW–SE direction of $\sigma 3$ based on striated fault sets. Our data coming from the dominant magma paths and the calculated major fault stress tensors, show that, at least during the Holocene, at Nisyros the NE-striking faults accommodated most of the normal slip, whereas ENE- to E–W-striking offshore faults could have had a left-lateral transcurrent component of motion. Our findings are thus compatible with the presence of a major offshore NE-trending graben, the prolongation of which crosses the Nisyros Island.

Based on all the aforementioned data, we suggest that the observable brittle structures inside the Nisyros caldera have not a typical radial pattern related to pure magma bulging, but instead they highlight a main NE–SW-trending zone of weakness that is geometrically controlled by the Quaternary regional tectonics.

6.3. Minor structures and magma bulging

The presence of some dispersion of the fault strikes within the caldera floor, which dominantly are N45–55° but range N45–80°, can reflect a secondary effect of magma bulging below the caldera controlled by regional structures, similar to what has been found in resurgent calderas (Bailey et al., 1976; Lipman, 1984; Self et al., 1986). This is consistent, for example, with the F7 faults that strike N80° and are clearly limited to the east by the main F1 and to the west by the western caldera ring fault (Fig. 13). Magma injection is facilitated along the main NE–SW weakness zone producing volcanoes whose location and shape is tectonically controlled. Some minor NW-striking faults and fractures found along the walls of the southwestern part of the caldera might be related to the development of the caldera ring faults, which here have the same strike. Based on the fact that several intracaldera faults terminate against the caldera ring faults, we wish to highlight the possible role of the latter that might act as boundary structures being also remobilised during deformation phases.

This interpretation can be compared with the results of Differential GPS and Differential Interferometric Synthetic Aperture Radar analyses made by Lagios et al. (2005); however, we highlight that their results are based on a six year monitored period (1997–2002), whereas our data show cumulative displacements in the order of the tens of thousands of years. Their data indicate that the total displacements ranged from 0.1 to 6 cm and from 3 to 15 cm for the horizontal and vertical components, respectively, and that the island was undergoing extension almost along the two major faulting zones F1 and F3 (Fig. 2). In the period 1996–1999, the ground surface uplifted with sub-circular interferometric fringes, but then subsided in 2000 with NE–SW-trending linear fringes. In agreement with these authors, we believe that the sub-circular uplift might have been induced by a magma chamber overpressure, and that the 2000 subsidence might have been controlled by the reactivation of the NE-striking F1 fault zone.

More evidence of a magma chamber located below the caldera is given by geochemical data: Increased H_2S/CO_2 ratios and decreasing CH_4/CO_2 ratios from the caldera fumaroles were caused by an increased contribution of the magmatic component to the recharge of the local hydrothermal system (Brombach et al., 2001). Moreover, the largest magmatic inputs occur below the main hydrothermal craters in the Lakki Plain (Chiodini et al., 2002; Brombach et al., 2003). Geophysical evidence based on Audio-Magnetotelluric measurements in the Nisyros geothermal field indicates two conductive bodies beneath about the centre of the island at a depth of 6–9 km (Dawes and Lagios, 1991; Lagios, 2000).

In a short time span (years), thus, it appears that uplift of the island, due to the overpressure of a magma chamber located at depth, is accommodated by doming without resulting in the formation of radial faults s.s. Deflation phases or the rest of doming phenomena are accompanied by deformation readjustments along the NE-striking fault system. In a longer time perspective, it seems that inflation/deflation phases of the magma chamber located below the caldera floor can be almost completely retrieved by the NE-striking faults. Possible stress loading along these planes can be readjusted due to long-term dilation induced by the extensional regional tectonics. Whatever incremental offsets along the NE-striking faults are produced by regional tectonics or magma inflation of a chamber located below the caldera, these causes cannot explain the complete extracaldera fault pattern, which is discussed in the next section.

6.4. The extracaldera fault pattern

Based on offset amount of stratigraphic units and on the scarp relief, the extracaldera NNW–SSE Mandraki Fault (F3) is one of the major structures at Nisyros. It strikes sub-perpendicularly to the more frequent NE-striking faults and fractures, although also showing dip-slip motions. The ENE–WSW-directed component of extension in the direction normal to F3 cannot easily be reconciled by the NW–SE regional direction of extension. Our field data indicate that the dip-slip motions along F3 have been produced by absolute uplift of the western block. This is based on the findings of several evidence of multiple stages of standing sea erosion levels which presently are located at altitudes from a few metres to 106 m a.s.l. This strong uplift is limited west of the Mandraki Fault, whereas the uplift magnitude rapidly decreases eastwards through step-like faults, among which a major role is played by F4. Southward, the geological record of uplift strongly decreases towards the NE-striking fault zones. The combination of these two main boundaries of uplift results in a tectonic block with a triangular shape in plan view and with an asymmetric uplift, larger northward (Fig. 13). This block corresponds also to the uplifted submarine basement of the island (Di Paola, 1974) and large and rapid uplift movements in the last 3–4 ky (Stiros, 2000, 2005). From a geological perspective, we found some record of a few metres of uplift also in the southern part of the island, but this very low amount clearly reflects the role of the NE-striking structures in confining the uplift. Our long-term findings are consistent with the short-term deformation calculated by Sachpazi et al. (2002) by SAR data, which is characterised by a maximum offset at the NW part of the island and a strong decrease at F1 and F3.

The bathymetric map shows the presence of a NNW-striking escarpment in correspondence of the seaward prolongation of the Mandraki Fault F3. Based also on the large offset measured along this fault on-land near to the coast line, we believe that it extends offshore for other 5 km, totalling 6.5 km in length. Other NNW-to NNE-striking faults have been detected offshore northwestern Nisyros, showing converging dips and delimitating a graben structure. N–S-trending linear features are also present along the western submerged flank of Nisyros volcano, whereas E–W-trending features are along the northern submerged flank. We interpret these lineaments as being the expression of faults. If we compare these data with the analogue experiments we conducted, it can be noticed that all the models portrayed in Fig. 12 show a similar fault pattern (i.e. an asymmetric hourglass-like structure). In the bathymetric map, the uphill-facing scarps of the E–W and N–S faults have a low relief because volcanic deposits and slope debris should have partially covered the scarps in onlap.

In the experiments, by locating the magma chamber in different positions with respect to the volcano model, we obtained other fault configurations that do not match the field data. Displacing the magma chamber further to the north, its inflation produces faults that do not reach the coastline, or that reach it with different geometry and kinematics. Although one could ague that a larger inflation might produce on-land propagation of faults, we highlight the fact that there would be a bias of geometry-kinematics. We thus believe that the best match of all the parameters between the scaled model and the prototype is reached with a magma chamber located 4.5 km NW of the caldera rim at a depth of 7.5–8.5 km.

By other methods, also Keller et al. (1990) support the existence of a large eruptive centre located between Nisyros and Kos. Dalabakis (1987) places a caldera with a diameter of at least 5–10 km between the volcanoes of Nisyros and Yali. Geophysical evidence also suggests the existence of this magma chamber located offshore: SAR data and seismological analysis from a seismological network indicate the presence of an aseismic area just south of Yali (5 km north of Nisyros), interpreted by Sachpazi et al. (2002) as the expression of a magma chamber. We agree that inflation of this chamber may be responsible for the unrest episode observed in 1995–1997 with uplift of the NW edge of Nisyros. The historic surface faulting observed on-land along the Mandraki Fault might

be the effect of magma overpressure in the chamber located offshore. The scissor-type movements here noticed should reflect the on-land slip that rapidly terminates near the fault tip, whereas most offset should have occurred offshore, in closer proximity to the magma chamber. The long series of uplift movements, and subsidence, which we detected on NW Nisyros, correspond to inflation-deflation phases of this magma chamber.

The NNE-striking faults (F5 and F6, Fig. 2), which we documented in the field along the N, NE and SW volcano flanks, resulted from a WNW–ESE $\sigma 3$ that matches neither the deformation of the Mandraki fault zone, nor that of the NE–SW main weakness zone. A distinction must be made between F5 and F6: F6 affect the older rock succession and show, at least locally, oblique slip (transtension) or even contraction (site 1 in Fig. 2). These could result from an older phase of deformation, consistent with the findings of Pe-piper et al. (2005) obtained at a more regional scale. The faults of F5, instead, offset a zone affected by younger deposits; their subvertical fault dip, the dip-slip normal motions and the fact that we have not found any evidence of a long-term uplift here, suggest that they might result from a combination of doming, due to the offshore magma chamber inflation phases, and regional tectonic deformation. In our opinion, F5 acts as an accommodation zone between the maximum uplift that occurs at the NW edge of the island, and the deformation that takes place during tectonic faulting along F1–F2 or the deflation phases (Fig. 13). The F5 faults thus might act under a double stress field: the one induced by magma overpressure that determines the complex hourglass fault system, and the one linked to the regional NW–SE $\sigma 3$.

7. Conclusions

- Our field data indicate that Nisyros island is affected by faults that, in the caldera zone, have different geometry and kinematics from the ones occurring at extracaldera zones. The caldera floor is affected by faults and fractures mostly striking NE–SW and ranging in strike from NE–SW to ENE–WSW. Extracaldera faults and fractures mostly strike NNW and NE. Most of the faults show normal motions, although transpressional deformations have been locally detected.
- On-land and offshore data suggest that the main NE-striking structures on Nisyros are consistent with NW–SE-directed tectonic extension, but they might move both under the tectonic regional stress state and under a local magma push. In this scenario, transient past phases of magma overpressure in a chamber located below the caldera can explain: (i) magma infilling of pre-existing fissures oriented perpendicularly to the regional NW–SE $\sigma 3$, (ii) uplift with a dominant dip-slip component of motions along the NE-striking faults in the caldera floor, and (iii) deformation along the caldera ring faults.
- Analogue modelling and field data indicate that the major normal, NNW-striking, extracaldera Mandraki Fault can be the expression of stress propagation from another magma chamber located immediately northwest of Nisyros.
- Considering the overall fault and fracture populations of northwestern Nisyros, their kinematics, and the offshore data, the best match of all the parameters between the scaled model and the prototype is reached with this second (offshore) magma chamber located 4.5 km NW of the caldera rim at a depth of 7.5–8.5 km.

Acknowledgements

We wish to thank E. Lekkas and B. van Wyk de Vries for their constructive and critical comments on a previous version of the manuscript, which greatly improved this work. This study has been funded by the Italian Ministry of University and Research (MIUR-PRIN). This is a contribution to the International Lithosphere Programme, Task II "New tectonic causes of volcano failure and possible premonitory signals".

References

Acocella, V., 2005. Modes of sector collapse of volcanic cones: Insights from analogue experiments. Journal of Geophysical Research 110, B02205, doi:10.1029/2004JB003166.
Acocella, V., Cifelli, F., Funiciello, R., 2000. Analogue models of collapse calderas and resurgent domes. Journal of Volcanology and Geothermal Research 104, 81–96.
Angelier, J., 1990. Inversion of field data in fault tectonics to obtain the regional stress—III. A new rapid direct inversion method by analytical means. Geophysical Journal International 103 (2), 363–376.
Apuani, T., Corazzato, C., Cancelli, A., Tibaldi, A., 2005. Physical and mechanical properties of rock masses at Stromboli: a dataset for flank instability evaluation. Bulletin of Engineering Geology and the Environment 64, 419–431, doi:10.1007/s10064-005-0007-0.
Bailey, R.A., Dalrymple, G.B., Lanphere, M.A., 1976. Volcanism, structure, and geochronology of Long Valley Caldera, Mono County, California. Journal of Geophysical Research 81, 725–744.
Bird, R.B., Stewart, W.E., Lighfoot, E.N., 1960. Transport Phenomena. John Wiley, New York, pp. 780.
Brombach, T., Caliro, S., Chiodini, G., Fiebig, J., Hunziker, J., Raco, B., 2003. Geochemical evidence for mixing of magmatic fluids with seawater, Nisyros hydrothermal system, Greece. Bulletin of Volcanology 65 (7), 505–516.
Caliro, S., Chiodini, G., Galluzzo, D., Granirei, D., La Rocca, M., Sacorotti, G., Ventura, G., 2005. Recent activity of Nisyros volcano (Greece) inferred from structural, geochemical and seismological data. Bulletin of Volcanology 67, 358–369.
Chadwick, W.W., Howard, K.A., 1991. The pattern of circumferential and radial eruptive fissures on the volcanoes of Fernandina and Isabela islands. Galapagos. Bulletin of Volcanology 53, 259–275.
Chadwick, W.W., Embley, R.W., Fox, C.G., 1995. SeaBeam depth changes associated with recent lava flows, CoAxial segment, Juan de Fuca ridge: Evidence for multiple eruptions between 1981-1993. Geophysical Research Letters 22 (2), 167–170.
Chiodini, G., Brombach, T., Caliro, S., Cardellini, C., Marini, L., Dietrich, V., 2002. Geochemical indicators of possible ongoing volcanic unrest at Nisyros Island (Greece). Geophysical Research Letters 29 (16), 1759, doi:10.1029/2001GL014355.
Corazzato, C., Tibaldi, A., 2006. Basement fracture control on type, distribution, and morphology of parasitic volcanic cones: an example from Mt. Etna, Italy. In: Tibaldi, A., Lagmay, M. (Eds.), Interaction between Volcanoes and their Basement. Journal of Volcanology and Geothermal Research, Special issue, 158, pp. 177–194.
Corti, G., Bonini, M., Mazzarini, F., Boccaletti, M., Innocenti, F., Manetti, P., Mulugeta, G., Sokoutis, D., 2002. Magma-induced strain localization in centrifuge models of transfer zones. Tectonophysics 348, 205–218.
Davis, E.N., 1967. Zur Geolofie und Petrologie der Inseln Nisyros und Jail (Dodekanes). Praktika of the Academy of Athens 42, 235–252.
Davison, I., Insley, M., Harper, M., Weston, P., Blundell, D., McClay, K., Quallington, A., 1993. Physical modelling of overburden deformation around salt diapers. Tectonophysics 228, 255–274.
Dawes, G.J.K., Lagios, E., 1991. A Magnetotelluric Survey of the Nisyros Geothermal Field (Greece). Geothermics 20 (4), 225–235.
Desio, A., 1931. Le isole italiane dell'Egeo. Memorie Carta Geologica d'Italia 24.
Di Paola, U., 1974. Volcanology and Petrology of Nisyros Island (Dodecannese,-Greece). Memorie dell'Istituto Geologico dell'Università di Padova 7.
Dixon, J.M., Simpson, D.G., 1987. Centrifuge modelling of laccolith intrusion. Journal of Structural Geology 9, 87–103.
Doutsos, T., Kokkalas, S., 2001. Stress and deformation patterns in the Aegean region. Journal of Structural Geology 23, 455–472.
Fytikas, M., Guliani, O., Innocenti, F., Marinelli, G., Mazzuoli, R., 1976. Geochronological data on recent magmatism of the Aegean sea. Tectonophysics 31, 29–34.
Gardeweg, M., Ramirez, C.F., 1987. La Pacana caldera and Atana Ignimbrite—A major ash flow and resurgent caldera complex in the Andes of northern Chile. Bulletin of Volcanology 49, 547–566.
Geotermica Italiana, 1983. Nisyros 1 geothermal well, PPC-EEC report, 160 pp.
Geotermica Italiana, 1984. Nisyros 2 geothermal well, PPC-EEC report, 44 pp.
Gudmundsson, A., 1988. Formation of collapse calderas. Geology 16, 808–810.
Gudmundsson, A., 1998. Formation and development of normal-fault calderas and the initiation of large explosive eruptions. Bulletin of Volcanology 60, 160–170.
Gudmundsson, A., 1999. Postglacial crustal doming, stresses and fracture formation with application to Norway. Tectonophysics 307, 407–419.
Hatzfeld, D., 1999. The present day tectonics of the Aegean as deduced from seismicity. In: Special Publication 156. Geological Society, London, pp. 416–426.
Henry, C., Price, J., 1989. The Christmas Mountains caldera complex. Trans-Pecos Texas: Bulletin of Volcanology 52, 97–112.
Hubbert, M., 1951. Mechanical basis for certain familiar geologic structures. Geological Society of America Bulletin 62, 355–372.
Jackson, J., 1994. Active tectonics of the Aegean region. Annual Review Earth Planetary Science 22, 239–271.

Johnson, C.A., Harrison, C.G.A., 1990. Neotectonics in central Mexico. Phys. Earth Planet. Inter. 64, 187–210.
Keller, J., Rehnen, T.H., Stadlbauer, E., 1990. Explosive volcanism in the Hellenic arc. A summary and review. In: Proceedings of the third scientific congress "Thera and the Aegean World III". Earth Sciences, vol. 2, pp. 13–26.
Kennedy, B., Stix, J., Vallance, J.W., Lavallée, Y., Longpré, M.-A., 2004. Controls on caldera structure: Results from analogue sandbox modeling. GSA Bulletin 116 (5/6), 515–524.
Komuro, H., Fujita, Y., Kodama, K., 1984. Numerical and experimental models on the formation mechanism of collapse basins during the Green Tuff Orogenisis of Japan. Bulletin of Volcanology 47, 649–666.
Komuro, H., 1987. Experiments on cauldron formation: A polygonal cauldron and ring fractures. Journal of Volcanology and Geothermal Research 31, 139–149.
Krantz, R.W., 1991. Normal fault geometry and fault reactivation in tectonic inversion experiments. In: Roberts (Ed.), The Geometry of Normal Faults. London Special Publication 56. Geological Society, pp. 219–229.
Lagabrielle, Y., Garel, E., Dauteuil, O., Cormier, M.-H., 2001. Extensional faulting and caldera collapse in the axial region of fast spreading ridges: Analog modeling. Journal of Geophysical Research 106 (B2), 2005–2015.
Lagios, E., 2000. Intense crustal deformation rates on Nisyros Island (Greece), deduced from GPS studies, may foreshadow a forthcoming volcanic event. In: Balassanian, S., Cisternas, A., Melkumyan, M. (Eds.), Proceedings of the 2nd International Conference on Earthquake Hazard and Seismic Risk Reduction. Kluwer, Dordrecht, pp. 249–259.
Lagios, E., Sakkas, V., Parcharidis, I., Dietrich, V., 2005. Ground deformation of Nisyros Volcano (Greece) for the period 1995–2002: Results from DInSAR and DGPS observations. Bulletin of Volcanology 68, 201–214, doi:10.1007/s00445-005-0004-y.
Lagmay, A.M.F., van Wyk de Vries, B., Kerle, N., Pyle, D.M., 2000. Volcano instability induced by strike-slip faulting. Bulletin of Volcanology 62, 331–346.
Limburg, E.M., Varekamp, J.C., 1991. Young pumice deposits on Nisyros, Greece. Bulletin of Volcanology 54, 68–77.
Lipman, P.W., 1984. The roots of ash flow calderas in Western North America: windows into the tops of granitic batholiths. Journal of Geophysical Research 89, 8801–8841.
Lipman, P.W., 1997. Subsidence of ash-flow calderas: Relation to caldera size and chamber geometry. Bulletin of Volcanology 59, 198–218.
Liritsis, I., Michael, C., Galloway, R., 1996. A significant Aegean volcanic eruption during the Second Millennium B.C. revealed by thermoluminescence dating. Geoarchaeology: An International Journal 11 (4), 361–371.
Lohrmann, J., Kukowski, N., Adam, J., Oncken, O., 2003. The impact of analogue materials proprieties on the geometry, kinematics, and dynamics of convergent sand wedges. Journal of Structural Geology 25, 1691–1711.
Mandl, G., 1988. Mechanics of tectonic faulting: models and basic concepts. Elsevier, Amsterdam, pp. 401.
Marini, L., Principe, C., Chiodini, G., Cioni, R., Fytikas, M., Marinelli, G., 1993. Hydrothermal eruptions of Nisyros (Dodecanese, Greece). Past events and present hazard. Journal of Volcanology and Geothermal Research 56, 71–94.
Martelli, A., 1917. Il gruppo eruttivo di Nisiro nel Mare Egeo. Memorie della Societa Italiano della Scienze detta dei XL Serie 3a T. XX.
Martí, J., Ablay, G.J., Redshaw, L.T., Sparks, R.S.J., 1994. Experimental studies of collapse calderas. Geological Society (London) Journal 151, 919–929.
Martí, J., Folch, A., Neri, A., Macedonio, G., 2000. Pressure evolution during explosive caldera-forming eruptions. Earth and Planetary Science Letters 175, 275–287.
McGuire, W.J., Pullen, A.D., 1989. Location and orientation of eruptive fissures and feeder-dykes at Mount Etna; influence of gravitational and regional tectonic stress regimes. Journal of Volcanology and Geothermal Research 38, 325–344.
Merle, O., Borgia, A., 1996. Scaled experiments of volcanic spreading. Journal of Geophysical Research 101 (B6), 13,805–13,817.
Mountrakis, D., 2005. Tertiary and Quaternary tectonics in Aegean area. In: Fytikas, M., Vougioualakis, G.E. (Eds.), The South Aegean Active Volcanic Arc. Elsevier, pp. 1–10.
Nakamura, K., 1977. Volcanoes as possible indicators of tectonic stress orientation - principle and proposal. Journal of Volcanology and Geothermal Research 2, 1–16.
Nappi, G., Renzulli, A., Santi, P., 1991. Evidence of incremental growth in the Vulsinian calderas (central Italy). Journal of Volcanology and Geothermal Research 47, 13–31.
Newhall, C., Dzurisin, D., 1988. Historical unrest at large calderas of the world: U.S. Geological Survey Bulletin 1855, 1–1108.
Nomikou, P., 2003. Santorini and Nisyros: Similarities and differences between the two calderas of the modern Aegean Volcanic Arc. In: Human Records of Recent Geological Evolution in the Mediterranean Basin—Historical and Archeological Evidence, Santorini, 22–25 October 2003 CIESM Workshop Monographs No. 24.
Nomikou, P., 2004. Geodynamic of Dodecanise islands: Kos and Nisyros volcanic field. PhD Thesis. Department of Geology, University of Athens.
Nomikou, P., Papanikolaou, D., 2000. Active geodynamics at Nisyros, the eastern edge of the aegean volcanic arc: emphasis on the submarine survey. Proceedings of the 3rd International Conference on the Geology of the Eastern Mediterranean, September 1998, 97–103.
Nordlie, B.E., 1973. Morphology and structure of the western Galapagos volcanoes and a model for their origin. Geological Society of America Bulletin 84, 2931–2956.
Papadopoulos, G.A., Sachpazi, M., Panopoulou, G., Stavrakakis, G., 1998. The volcano-seismic crisis of 1996–97 in Nisyros, SE Aegean Sea, Greece. Terra Nova 10, 151–154.
Papanikolaou, D., Lekkas, E.L., Sakelariou, D., 1991. Volcanic stratigraphy and evolution of the Nisyros volcano. Bulletin of the Geological Society of Greece 25, 405–419.
Papanikolaou, D., Nomikou, P., 2001. Tectonic structure and volcanic centres at the eastern edge of the Aegean Volcanic Arc around Nisyros island. Proceedings of the 9th International Congress, Athens, September 2001. Bulletin of the Geological Society of Greece XXXIV (1), 289–296.
Papanikolaou, D., 1993. Geotectonic evolution of the Aegean. Bulletin of the Geological Society of Greece 28 (1), 33–48.
Papazachos, B.C., Karakostas, V.G., Papazachos, C.B., Scordilis, E.M., 2000. The geometry of the Wadati-Benioff zone and lithospheric kinematics in the Hellenic arc. Tectonophysics 319, 275–300.
Papazachos, B.C., Dimitriadis, S.T., Panagiotopoulos, D.G., Papazachos, C.B., Papadimitriou, E.E., 2005. Deep structure and active tectonics of the southern Aegean volcanic arc. In: Fytikas, M., Vougioualakis, G.E. (Eds.), The South Aegean Active Volcanic Arc. Elsevier, pp. 47–64.
Pasquarè, F.A., Tibaldi, A., 2003. Do transcurrent faults guide volcano growth? The case of NW Bicol Volcanic Arc, Luzon, Philippines. Terra Nova 15, 204–212.
Pavlakis, P., Lykoussis, V., Papanikolaou, D., Chronis, G., 1990. Discovery of a new submarine volcano in the western Saronic Gulf: The Paphsanias Volcano. Bulletin of the Geological Society of Greece 24, 59–70.
Pe-Piper, G., Piper, D.J.W., 2005. The South Aegean Active Volcanic Arc: Relationships between magmatism and tectonics. In: Fytikas, M., Vougioukalakis, G.E. (Eds.), The South Aegean Active Volcanic Arc. Elsevier, pp. 113–133.
Pe-Piper, G., Piper, D.J.W., Perissoratis, C., 2005. Neotectonics of the Kos Plateau Tuff eruption of 161 ka, South Aegean Sea. Journal of Volcanology and Geothermal Research 139, 315–338.
Phillips, W.J., 1974. The dynamic emplacement of cone sheets. Tectonophysics 24, 69–84.
Piper, D.J.W., Perissoratis, C., 2003. Quaternary neotectonics of the South Aegean arc. Marine Geology 198, 259–288.
Pollard, D.D., Aydin, A., 1988. Progress in understanding jointing over the past century. Geological Society of America Bulletin 100, 1181–1204.
Ramberg, H., 1981. Gravity, deformation and the earth's crust, 2nd ed. Academic Press, London, pp. 452.
Reynolds, R.W., Geist, D., Kurz, M.D., 1995. Physical volcanology and structural development of Sierra Negra volcano, Isabela Island, Galapagos Archipelago. Geological Society of America Bulletin 107, 1398–1410.
Roman-Berdiel, T., Gapais, D., Brun, J.P., 1995. Analogue models of laccolith formation. Journal of Structural Geology 17, 1337–1346.
Roche, O., Druitt, T., Merle, O., 2000. Experimental study of caldera formation. Journal of Geophysical Research 105, 395–416.
Sachpazi, M., Kontoes, Ch., Voulgaris, N., Laigle, M., Vougioukalakis, G., Olga Sikioti, G., Stavrakakis, G., Baskoutas, J., Kalogeras, J., Lepine, J.Cl., 2002. Seismological and SAR signature of unrest at Nisyros caldera, Greece. Journal of Volcanology and Geothermal Research 116, 19–33.
Sakkas, V., Lagios, E., Parcharidis, I., Vassilopoulou, S., 2002. Surface displacement model of Nisyros volcanic field deduced from DInSAR analysis & DGPS Measurements. Proceedings of the 11th General Assembly of Wegener Project, September 2002, Athens, Greece.
Saotome, A., Yoshinaka, R., Osada, M., Sugiyama, H., 2002. Constituent material properties and clast-size distribution of volcanic breccia. Engineering Geology 64, 1–17.
Self, S., Goff, F., Gardner, J.N., Wright, J.V., Kite, W.M., 1986. Explosive rhyolitic volcanism in the Jemez Mountains: vent locations, caldera development and relation to regional structure. Journal of Geophysical Research 91, 1779–1798.
Schultz-Ela, D.D., Jeckson, M.P.A., Vendeville, B.C., 1993. Mechanics of active salt diapirism. Tectonophysics 228, 275–312.
Smith, R., Bailey, R., 1968. Resurgent cauldrons, in: Studies in Volcanology: A Memoir in Honor of Howel Williams. Geological Society of America Memoir 116, 83–104.
Stiros, S., McGuire, W.J., Griffiths, D.R., Hancock, P.L., Stewart, I.S., 2000. Fault pattern of Nisyros Island Volcano (Aegean Sea, Greece); structural, coastal and archaeological evidence. In: The Archaeology of Geological Catastrophes. Geological Society Special Publications, 171, pp. 385–397.
Stiros, S., 2005. Late-Holocene coastal uplift in the Nisyros volcano (SE Aegean Sea): Evidence for a new phase of slow intrusive activity. In: Fytikas, M., Vougioukalakis, G.E. (Eds.), The South Aegean Active Volcanic Arc. Elsevier, pp. 217–225.
Strecker, M., Bosworth, W., 1991. Quaternary stress field change in the Gregory Rift, Kenya. EOS Transactions American Geophysical Union 72, 17–22.
Tibaldi, A., 1995. Morphology of pyroclastic cones and tectonics. Journal of Geophysical Research 100 (24), 521–524. 535.
Tibaldi, A., 1996. Non-tectonic faulting: examples from late Quaternary trachytes of Ischia Island and basalts of Mt. Etna, Italy. Acta Vulcanologica 8 (1), 91–98.
Tibaldi, A., Groppelli, G., 2002. Volcano-tectonic activity along the structures of the unstable NE flank of Mt. Etna, Italy. Journal of Volcanology and Geothermal Research 115 (3-4), 277–302.
Tibaldi, A., Bistacchi, A., Pasquare, F.A., Vezzoli, L., 2006. Extensional tectonics and volcano lateral collapses: insights from Ollague volcano (Chile-Bolivia) and analogue modelling. Terra Nova 18 (4), 282–289, doi:10.1111/j.1365-3121.2006.00691.x.
Tibaldi A., Pasquarè F.A., Papanikolaou D., Nomikou P., in press. Discovery of a huge sector collapse at the Nisyros caldera, Greece, by onshore and offshore geological-structural data. Journal Volcanology and Geothermal Research.
Troll, V.R., Walter, T.R., Schmincke, H.-U., 2002. Cyclic caldera collapse: Piston or piecemeal subsidence? Field and experimental evidence. Geology 30 (2), 135–138.
Turcotte, D.L., Schubert, G., 1982. Geodynamics: application of continuum physics to geological problems. Wiley, New York, pp. 450.

Vanderkluysen, L., Volentik, A.C.M., Principe, C., Hunziker, J.C., Hernandez, J., 2005. Nisyros' volcanic evolution: the growth of a strato-volcano. In: Hunziker, J.C., Marini, L. (Eds.), The Geology Geochemistry and Evolution of Nisyros Volcano (Greece) Implications for the Volcanic Hazards. Mémoires de Géologie (Lausanne), 44, pp. 100–106.

Varnes, D., 1963. Geology and Ore Deposits of the South Silverton Mining Area, San Juan County, Colorado. U.S. Geological Survey Professional Paper 378-A, 1–56.

Vidal, N., Merle, O., 2000. Reactivation of basement faults beneath volcanoes: a new model of flank collapse. Journal of Volcanology and Geothermal Research 99, 9–26.

Volentik, A,, Vanderkluysen, L., Principe, C., Hunziker, J.C., 2005. Stratigraphy of Nisyros volcano (Greece). In: Hunziker, J.C., Marini, L. (Eds.), The Geology, Geochemistry and Evolution of Nisyros Volcano (Greece). Implications for the Volcanic Hazards. Mémoires de Géologie (Lausanne), 44, pp. 26–67. ISSN 1015-3578.

Vougioukalakis, G., 1993. Volcanic stratigraphy and evolution of Nisyros island. Bulletin of the Geological Society of Greece 28, 239–258.

Walter, T.R., Troll, V.R., 2001. Formation of caldera periphery faults, an experimental study. Bulletin of Volcanology 63, 191–203.

Weijermars, R., Schmeling, H., 1986. Scaling of Newtonian and non Newtonian fluid dynamics without inertia for quantitative modelling of rock flow due to gravity (including the concept of rheological similarity). Physics of the Earth and Planetary Interiors 43, 316–330.

Withjack, M.O., Scheiner, C., 1982. Fault patterns associated with domes: An experimental and analytical study. AAPG Bulletin 66, 302–316.